Ore Geology Reviews 89 (2017) 822–835

Contents lists available at ScienceDirect

Ore Geology Reviews

journal homepage: www.elsevier.com/locate/oregeorev

Magnetite geochemistry of the Longqiao and Tieshan Fe–(Cu) deposits in the Middle-Lower Yangtze River Belt: Implications for deposit type and ore genesis

Xia Hu[a,b], Huayong Chen[a,c,*], Liandang Zhao[a,b], Jinsheng Han[a], Xiaoping Xia[d]

[a] Key Laboratory of Mineralogy and Metallogeny, Guangzhou Institute of Geochemistry, Chinese Academy of Sciences, Guangzhou 510640, China
[b] Graduate University of Chinese Academy of Sciences, Beijing 100049, China
[c] State Key Laboratory of Ore Deposit Geochemistry, Institute of Geochemistry, Chinese Academy of Sciences, Guiyang 550002, China
[d] State Key Laboratory of Isotope Geochemistry, Chinese Academy of Sciences, Guangzhou 510640, China

ARTICLE INFO

Keywords:
Magnetite chemistry
Longqiao Fe deposit
Tieshan Fe–(Cu) deposit
Skarn
Middle–Lower Yangtze River Belt (MLYRB
Eastern China)

ABSTRACT

Magnetite is a common mineral in many ore deposits and their host rocks, and contains a wide range of trace elements (e.g., Ti, V, Mg, Cr, Mn, Ca, Al, Ni, Ga, Sn) that can be used for deposit type fingerprinting. In this study, we present new magnetite geochemical data for the Longqiao Fe deposit (Luzong ore district) and Tieshan Fe–(Cu) deposit (Edong ore district), which are important magmatic-hydrothermal deposits in eastern China.

Textural features, mineral assemblages and paragenesis of the Longqiao and Tieshan ore samples have suggested the presence of two main mineralization periods (sedimentary and hydrothermal) at Longqiao, among which the hydrothermal period comprises four stages (skarn, magnetite, sulfide and carbonate); whilst the Tieshan Fe–(Cu) deposit comprises four mineralization stages (skarn, magnetite, quartz-sulfide and carbonate).

Magnetite from the Longqiao and Tieshan deposits has different geochemistry, and can be clearly discriminated by the Sn vs. Ga, Ni vs. Cr, Ga vs. Al, Ni vs. Al, V vs. Ti, and Al vs. Mg diagrams. Such difference may be applied to distinguish other typical skarn (Tieshan) and multi-origin hydrothermal (Longqiao) deposits in the MLYRB. The fluid–rock interactions, influence of the co-crystallizing minerals and other physicochemical parameters, such as temperature and fO_2, may have altogether controlled the magnetite trace element contents of both deposits. The Tieshan deposit may have had higher degree of fO_2, but lower fluid–rock interactions and ore-forming temperature than the Longqiao deposit. The TiO_2–Al_2O_3–(MgO + MnO) and (Ca + Al + Mn) vs. (Ti + V) magnetite discrimination diagrams show that the Longqiao Fe deposit has both sedimentary and hydrothermal features, whereas the Tieshan Fe–(Cu) deposit is skarn-type and was likely formed via hydrothermal metasomatism, consistent with the ore characteristics observed.

1. Introduction

Magnetite is a common mineral in many igneous, metamorphic and sedimentary rocks, as well as in various Fe-dominated deposit-types, including Kiruna-type, BIF (banded iron formation), magmatic Fe-Ti oxide, Fe-skarn (Dupuis and Beaudoin, 2011; Huberty et al., 2012; Nadoll et al., 2012), IOCG (iron oxide–copper–gold) and porphyry deposits (Liang et al., 2009; Williams et al., 2005). Magnetite can form in a wide range of temperatures and hosts a variety of foreign cations, such as Mg, Al, Ti, V, Cr, Ni, Si, Ca, and Mn (Dupuis and Beaudoin, 2011; Nadoll et al., 2014a; Dare et al., 2012), and has been the focus for many magnetite-bearing mineral systems in recent years (Chen et al., 2015a,b; Chung et al., 2015; Hu et al., 2015; Huang et al., 2015a,b; Makvandi et al., 2015; Zhao and Zhou, 2015; Zhao et al., 2016; Canil et al., 2016). Previous studies have shown that compositional variety in magnetite can be used for geochemical fingerprinting of deposit types (Carew, 2004; Singoyi et al., 2006; Rusk et al., 2009; Dupuis and Beaudoin, 2011; Dare et al., 2012; Nadoll et al., 2012): For instance, magnetite grains from skarn deposits generally have lower Ti and V, but higher Ca, Al, and Mn, than those from Kiruna-type and magmatic Fe–Ti oxide deposits (Dupuis and Beaudoin, 2011). The types and concentrations of trace elements in magnetite are mainly controlled by physicochemical parameters of the ore-forming system, such as fluid compositions, temperature (T), pressure (P), cooling rate, oxygen (fO_2) and sulfur (fS_2) fugacity (Nadoll et al., 2012). Thus, magnetite geochemistry can reflect T–P–fO_2 conditions of the ore-forming system

* Corresponding author at: Guangzhou Institute of Geochemistry, Chinese Academy of Sciences, P.O. Box 1131, Tianhe District, Guangzhou 510640, Guangdong, China.
E-mail address: huayongchen@gig.ac.cn (H. Chen).

http://dx.doi.org/10.1016/j.oregeorev.2017.07.019
Received 27 December 2016; Received in revised form 19 June 2017; Accepted 23 July 2017
Available online 25 July 2017
0169-1368/

(Nystroem and Henriquez, 1994; Toplis and Corgne, 2002; Carew, 2004; Dare et al., 2014; Dupuis and Beaudoin, 2011; Nadoll et al., 2012, 2014a,b).

The Middle–Lower Yangtze River Belt (MLYRB) in eastern China is one of the most important Cu–Fe–Au–Mo mineralization belts in China. The Luzong and Edong ore clusters are important Fe ore districts of the MLYRB (Fan et al., 2011, 2014; Zeng et al., 2010; Li et al., 2013; Ma et al., 2011; Zhou et al., 2011, 2010; Duan et al., 2011; Chen et al., 2012; Zhang et al., 2014), yet the deposit type and ore genesis of some deposits are still controversial, e.g., the Longqiao Fe deposit (Luzong ore district) and the Tieshan Fe–(Cu) deposit (Edong ore district).

The Longqiao Fe deposit is one of the most important deposits in the Luzong ore district (120 Mt at 44% Fe, Wu, 1996). Previously, Li et al. (2013) had constrained the mineralization age using the phlogopite ^{40}Ar–^{39}Ar age of 147.13 ± 1.45 Ma. Duan et al. (2009) concluded that the mineralization was associated with the early-Middle Triassic sedimentary process and Cretaceous (late Yanshanian) hydrothermal event. Ren et al. (1991) suggested that the deposit was closely associated with volcanic exhalative sedimentary processes, whereas Ni et al. (1994) argued that the deposit was formed by exhalative sedimentary hydrothermal overprinting on a pre-existing Fe deposit. More recently, Zhou et al. (2011) considered that the Longqiao deposit is a skarn-type stratabound mineral system.

The Tieshan Fe–(Cu) deposit is a very important deposit in the Edong ore district (160 Mt at 53% Fe, 0.67 Mt at 0.58% Cu, Yao et al., 1993). Previous research investigating the Tieshan magnetite texture and geochemistry yielded different conclusions, e.g., Zhai et al. (1982) considered that the Tieshan Fe–(Cu) deposit was formed by injected ore magma. Zhao (1990) concluded that the Tieshan deposit is primarily a Mg skarn–type deposit; Duan et al. (2014) suggested a hydrothermal metasomatism origin instead of magmatic; Hu et al. (2015) argued that Tieshan is a Fe-skarn-type deposit and its magnetite was re-equilibrated by dissolution and re-precipitation; Wang et al. (2015) suggested that Tieshan comprises both magmatic- and hydrothermal- type ores. However, little geochemical comparison was made between magnetite from the Tieshan Fe–(Cu) deposit and other Fe deposits in MLYRB.

In this paper, we present new geological descriptions and EMPA and LA-ICP-MS chemical data of magnetite from the Longqiao Fe and Tieshan Fe (-Cu) deposits. We also compare the geochemical characteristics of the Longqiao and Tieshan magnetite with other Fe deposits in MLYRB, and discuss the deposit type and genesis of magnetite.

2. Regional and deposit geology

The MLYRB contains seven important Fe–(Cu) ore districts. From west to east, these are the Edong, Jiurui, Anqing–Guichi, Luzong, Tongling, Ningwu, and Ningzhen districts, which extend along the northern margin of the Yangtze Craton and the southeastern margin of the North China Craton, and the Dabieshan Orogenic Belt. The MLYRB is bounded by the Xiangfan–Guangji Fault (XGF) to the northwest, the regional strike-slip Tancheng–Lujiang Fault (TLF) to the northeast, and the Yangxin–Changzhou Fault (YCF) to the south (Fig. 1). The three major tectonostratigraphic units of the MLYRB are the Archean–Proterozoic metamorphic basement, Cambrian to Middle Triassic submarine sediments, and Middle Triassic to Cretaceous terrigenous clastic and volcanic rocks (e.g., Zhai et al., 1992, 1996).

2.1. The Longqiao Fe deposit

The Mesozoic Luzong volcanic basin is in the central part of the MLYRB (Fig. 1). The basin is controlled by the Tancheng–Lujiang Fault (TLF) and the Yangtze River Fault (Fig. 2a) (Li et al., 2013; Zhou et al., 2010). The basin basement comprises Middle–Lower Jurassic continental clastic sediments and upper Triassic marine and terrigenous clastics and carbonates. Mesozoic (Yanshanian) shoshonitic volcanics are abundant in the Luzong basin (Ren et al., 1991; Sun et al., 1994; Wang et al., 2006; Xue et al., 2010), and comprise (from oldest to youngest) the Longmenyuan (K_{1l}), Zhuanqiao (K_{1z}), Shuangmiao (K_{1s}) and Fushan (K_{1f}) formations (Zhou et al., 2011). These four formations are exposed in a ring-shaped zone, with the Fushan Formation in the center and the Longmenyuan Formation in the rim. The Zhuanqiao, Shuangmiao, Fushan and Longmenyuan Formation comprise mainly pyroxene trachyandesite, trachybasalt, trachyte and trachyandesite, respectively (Zhou et al., 2008a). Major intrusive rock types include diorite, monzonite, granite and syenite (Zhou et al., 2008b).

The Longqiao Fe deposit is located in the northern Luzong basin (Fig. 2a). Exposed stratigraphy comprises mainly the Dongma'anshan (T_{2d}), Luoling (J_{2l}), Longmenyuan (K_{1l}) and Zhuanqiao (K_{1z}) formations (pyroxene)-trachyandesite (Fig. 2b).

The principal mineral commodity of the Longqiao Fe deposit is magnetite. The Longqiao Fe deposit has a resource of 120 Mt iron ore at 44% Fe (Wu, 1996). The deposit is stratiform or stratoid, reaches depths of 400 to 50 m. The orebodies are hosted in marl, calcite dolomite, breccia limestone, breccia dolomitic limestone and pelitic siltstone of the Dongma'anshan Formation (Tang, 1998; Wu, 1996). The hanging wall comprises mainly the Dongma'anshan Formation pelitic siltstone and local Longmenyuan Formation trachyandesite, whilst the footwall comprises the Dongma'anshan Formation pelitic siltstone intruded by syenite (Zhou et al., 2011). Magnetite ores at Longqiao are commonly massive, disseminated or laminated, and locally occur as lumps, breccia or mesh-like. Ore textures include hypidiomorphic-xenomorphic granular, euhedral granular, xenomorphic-granular, skeletal, poikilitic and foliated. Minor lamellar ores (enclosed by massive ores) are also found in the upper part of the orebody, which have been interpreted as evidence for a sedimentary origin (Ni et al., 1994; Tang, 1998; Wu, 1996). Metallic minerals include mainly magnetite and minor pyrite, siderite and chalcopyrite. Diopside, garnet, and calcite are the dominant gangue minerals. Wall rock alteration at Longqiao is well developed and comprises six alteration zones, i.e., (from top to bottom) K-feldspar–kaolinite–chlorite, K-feldspar–tourmaline, skarn, alkali-feldspar–hornfels and hornfels (Wu, 1996).

2.2. The Tieshan Fe–(Cu) deposit

The Edong ore district (southeastern Hubei Province) is situated in the westernmost MLYRB (Fig. 1). Exposed strata include mainly the Triassic Daye Formation carbonates and Puqi Formation sandy-shale, the Jurassic Wuchang Formation coal-bearing sandy-shale, Ziliujin Formation arenite, Lingxiang Formation and Dasi Formation volcanic and pyroclastic rocks (Xie et al., 2012, 2015). Among these formations, the Daye Formation marble and Puqi Formation sandy-shale are the major ore-hosting rocks for the Fe–Cu skarn mineralization in this area. The Edong ore district is mainly controlled by ENE-trending faults (Shu et al., 1992), and contains widespread Jurassic–Cretaceous intermediate-felsic intrusions, e.g., (from north to south) E'cheng, Tieshan, Jinshandian, Yangxin, Lingxiang and Yinzu. This district is well-endowed with many Fe, Fe–Cu–(Au), Cu–Au and Cu–Mo–(W) skarn or porphyry deposits (Fig. 3a), which were interpreted to be related to Yanshanian intermediate-felsic intrusive rocks. From southeast to northwest, metals zoning of W–Cu–Mo → Cu-Mo → Cu → Fe-Cu → Fe was reported (Shu et al., 1992).

The Tieshan Fe–(Cu) deposit in the northwestern Edong district (Fig. 3a) hosts proven reserves of 160 Mt Fe (53%) and 0.67 Mt Cu (0.58%) (Yao et al., 1993), as well as economic Co, Ni, Au, and Ag. Exposed strata include the Upper Permian Dalong and Longtan formations and the Lower Triassic Daye Formation carbonatite and pelite. The deposit is related to the Early Cretaceous Tieshan intrusive complex that intruded the Daye Formation marine carbonates. The Tieshan complex consists of syenodiorite, diopside diorite, monzodiorite, granodiorite and quartz diorite. The Tieshan deposit contains six major lenticular or podiform orebodies (Tiemenkan, Longdong, Jianlinshan, Xiangbishan, Shizishan and Jianshan) located predominantly along the

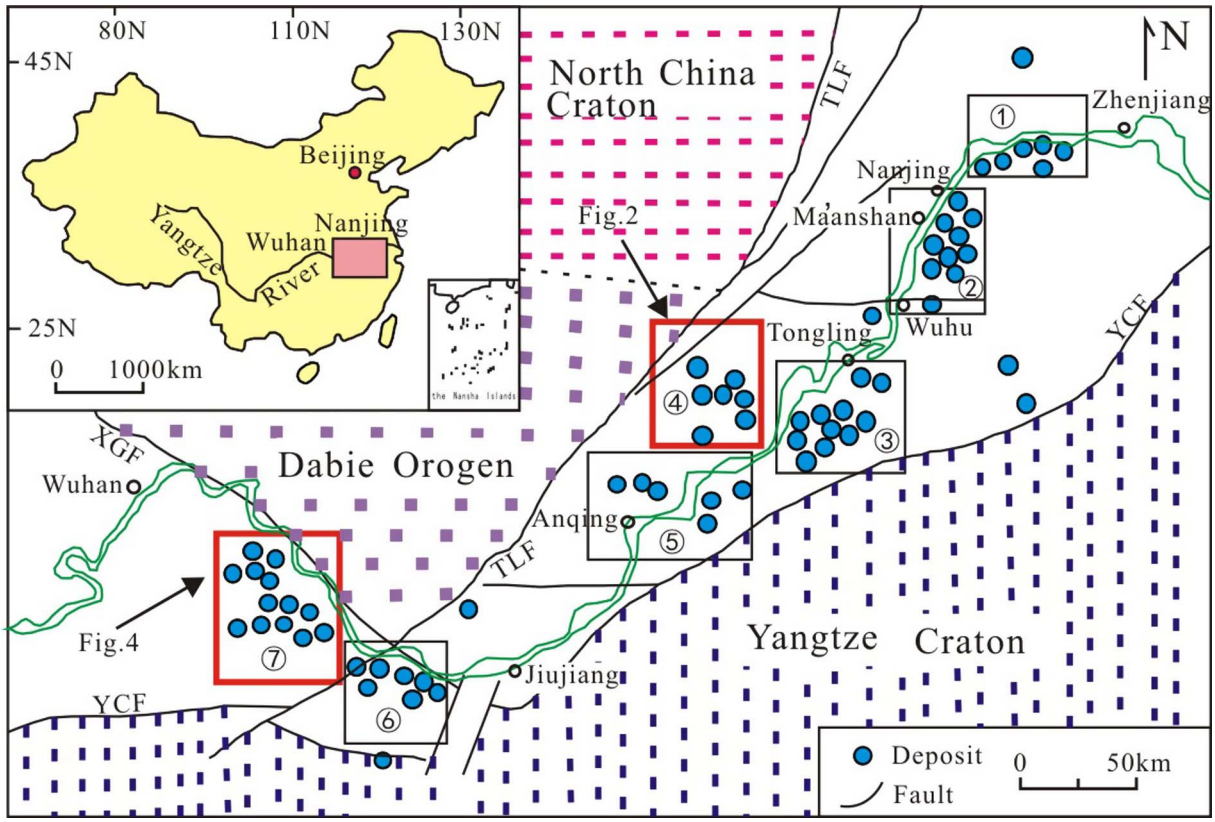

Fig. 1. Sketch map showing the distribution of main metallogenic districts and deposits in the Middle–Lower Yangtze River Valley Belt (modified after Zhou et al., 2010). ①Ningzhen ore district; ②Ningwu ore district; ③Tongling ore district; ④Luzong ore district; ⑤Anqing-Guichi ore district; ⑥Jiurui ore district; ⑦Edong ore district.

marble–quartz diorite contact (Fig. 3b). Metallic minerals include mainly magnetite and minor pyrite, chalcopyrite, pyrrhotite and hematite. The gangue minerals are mainly diopside, garnet, phlogopite, amphibole, chlorite and calcite. Wall rock alteration is locally well developed at Tieshan, with the main types include skarn, sodic, potassic, silicic, carbonate and chlorite alterations (Qu et al., 2012).

3. Paragenesis and mineralization stages

Representative Fe ore samples from Longqiao and Tieshan were prepared as polished thin sections and subsequently examined using optical microscopy to characterize the textural and mineralogical features.

3.1. Paragenesis of the Longqiao Fe deposit

Based on the previous studies (e.g., Zhou et al., 2011) and our observations, the Longqiao mineralization comprises two periods (sedimentary and hydrothermal), and the hydrothermal period consists of four stages (skarn, magnetite, sulfide and carbonate) (Fig. 4).

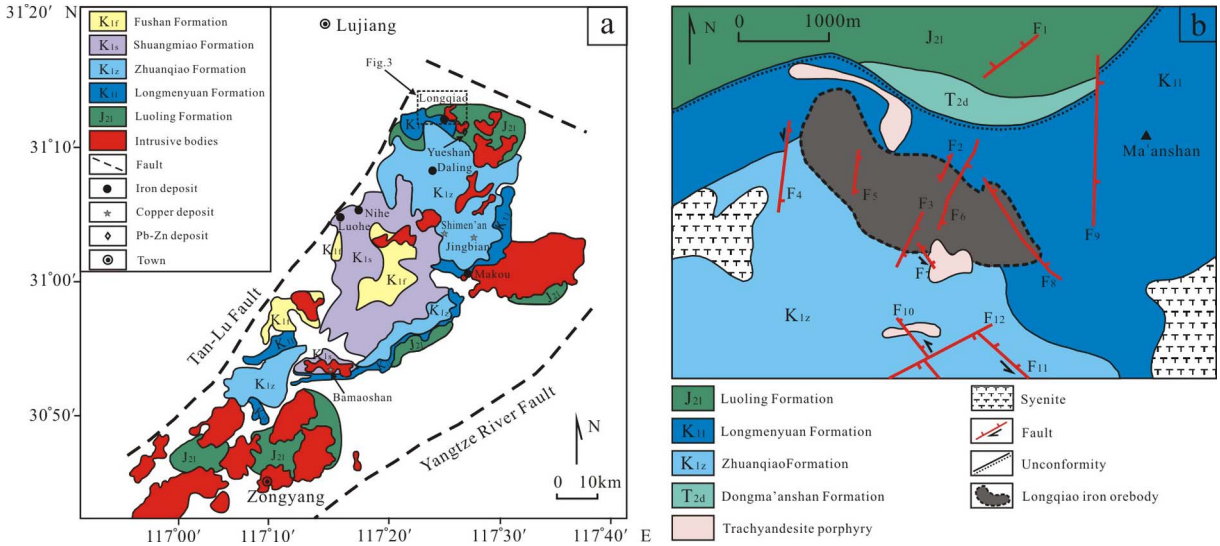

Fig. 2. Simplified geologic map of (a) the Luzong ore district; (b) the area around the Longqiao Fe deposit (the Longqiao iron orebody was a projection to surface). Modified after Zhou et al. (2011).

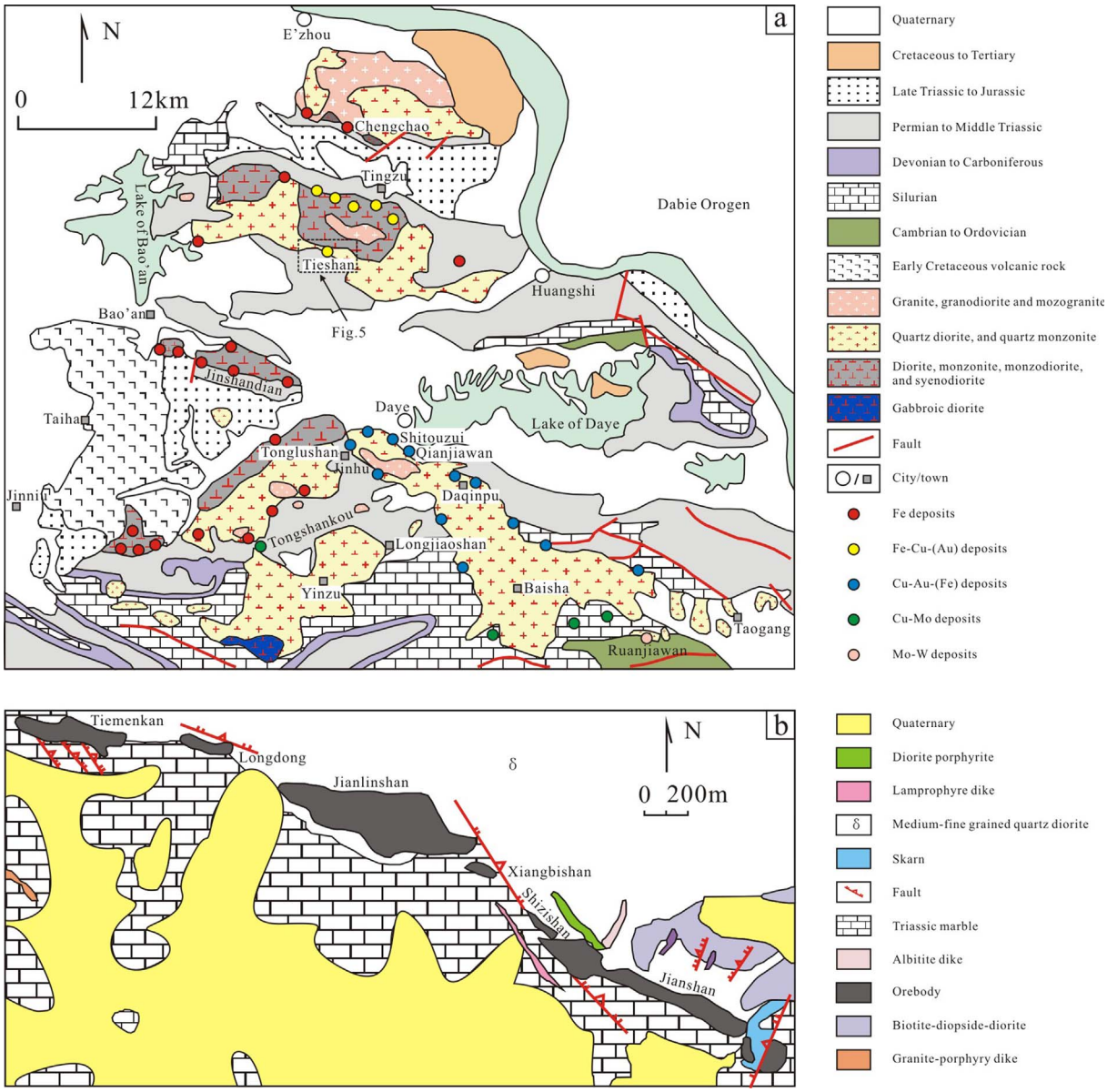

Fig. 3. Simplified geologic map of (a) the Edong ore district (modified after Hu et al., 2014a,b); (b) the Tieshan Fe–Cu deposit (modified after Shen et al., 2012).

The sedimentary period contains mainly siderite, quartz, calcite, and minor gypsum, ankerite, hematite, barite and anhydrite. This period mainly hosts laminated ores with a light-colored band which mainly consists of silicate minerals and a black band which mainly comprises magnetite. Under the microscope, we can see that siderite is commonly subhedral, colorless, and is locally replaced by skeletal magnetite (Zhou et al., 2011).

The skarn stage contains mainly wollastonite, diopside and garnet and minor K-feldspar, tourmaline, chlorite, epidote, amphibole and magnetite. Under the microscope, we can see that wollastonite is crosscut by epidote (Fig. 5a). The magnetite stage is the main Fe mineralization stage and contains mainly magnetite, quartz, and hematite, with minor tourmaline, serpentine, epidote and chlorite. This stage hosts mainly massive magnetite ores (Fig. 5b). We observed that magnetite crosscut barite (Fig. 5c). In addition, magnetite is closely associated with quartz and hematite (Fig. 5d), and is commonly crosscut by late sulfides (Fig. 5e). The sulfide stage is dominated by pyrite and chalcopyrite, with minor calcite, hematite, chlorite, galena, sphalerite and kaolinite. Chalcopyrite is associated with calcite and hematite (Fig. 5f). The carbonate stage is dominated by late carbonate veins crosscutting or infilling the older minerals, e.g., magnetite and quartz (Fig. 5d, e).

3.2. Paragenesis of the Tieshan Fe–(Cu) deposit

Combining the textural and structural features, mineral assemblages and cross-cutting relationships of ore samples with previous studies, the Tieshan Fe–(Cu) deposit mineralization can be divided into four stages: 1) skarn, 2) magnetite, 3) quartz-sulfide and 4) carbonate (Fig. 6, Xie et al., 2006; Qu et al., 2012).

The skarn stage contains mainly garnet and diopside, and minor epidote. Diopside is mostly replaced by phlogopite along its margins or fractures (Fig. 7a). The magnetite stage is the main Fe mineralization stage, in which magnetite is commonly intergrown with phlogopite (Fig. 7a). Amphibole veins crosscut magnetite and diopside (Fig. 7b), suggesting that amphibole post-dates Fe mineralization. Locally, phlogopite and amphibole are chlorite altered. The quartz–sulfide stage is the main Cu mineralization stage, and contains mainly quartz, pyrite, chalcopyrite and minor pyrrhotite (Fig. 7c). Pyrite and chalcopyrite veins crosscut magnetite (Fig. 7c). The carbonate stage is dominated by

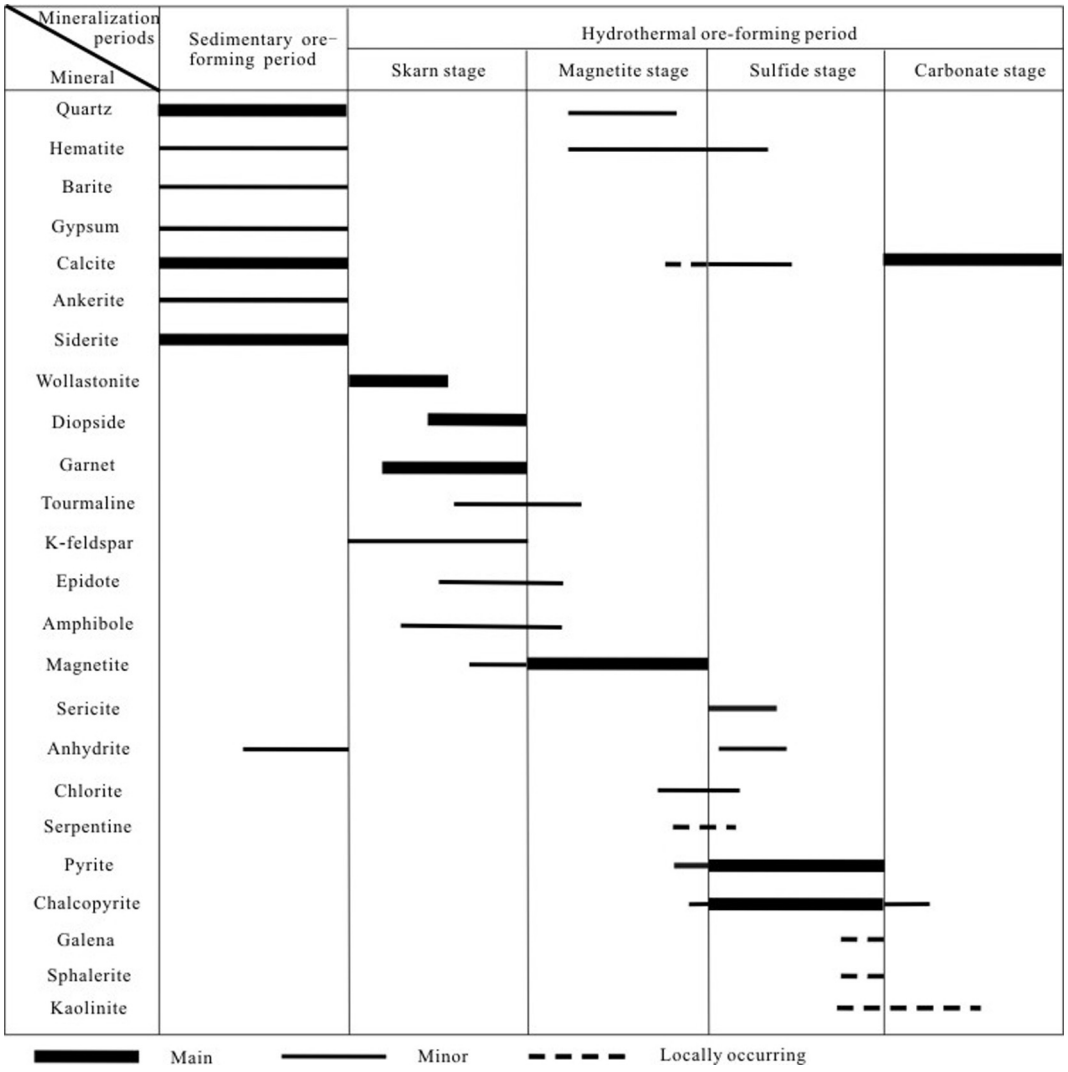

Fig. 4. Mineralization paragenesis of the Longqiao Fe deposit (modified after Zhou et al., 2011).

calcite, chlorite and hematite. Magnetite is commonly crosscut by calcite veins, and replaced by hematite along fissures (Fig. 7d).

4. Sample analytical methods and results

4.1. Analytical methods

Ten representative samples were selected for the magnetite geochemical analyses. All these samples are from the magnetite stage. Among them, sample LQ-2, LQ-4, LQ-5, LQ-6, LQ-7 and LQ-8 are from the Longqiao Fe deposit. Sample TS-78-2, TS-122, TS-150-1, TS-136 and TS-200 are from the Tieshan Fe–(Cu) deposit. The samples were prepared as polished thin sections and carbon-coated for electron probe microanalysis (EPMA) and laser ablation-inductively coupled plasma-mass spectrometry (LA-ICP-MS) analyses.

Major elements of magnetite were determined using a JEOL-JAX-8100 electron probe in the Electron Probe Laboratory of the Guangzhou Institute of Geochemistry, Chinese Academy of Sciences (GIG-CAS). The analyses were carried out with 15 kV voltage, 20 nA beam current and 5 μm spot size. Relative standard deviation was below 0.01%.

Trace elements of magnetite were analyzed by a pulsed Resonetic 193 nm laser ablation system coupled with an Agilent 7500a ICP-MS at the GIG-CAS. Detailed LA-ICP-MS operating conditions and data reduction were described in Liu et al. (2008). Helium was applied as a carrier gas, mixed with argon (as the makeup gas) via a T-connector before entering the ICP. Analytical spots (23 μm) were ablated by 160 successive laser pulses (4 Hz). Each analysis included a background acquisition of approximately 20 s for a gas blank, followed by data acquisition of 40 s for the sample. Element contents were calibrated against reference material (BHVO-2G) using ^{57}Fe as the internal standard (Liu et al., 2008). Every five sample analyses were followed by one analysis of BHVO-2G to correct the time-dependent drift of sensitivity and mass discrimination. Off-line selection and integration of background and analytical signals, and time drift correction and quantitative calibration were performed using ICPMSDataCal (Liu et al., 2008).

4.2. Analytical results

4.2.1. EPMA

Results of EPMA for the Longqiao and Tieshan magnetite are presented in Table 1. The Longqiao and Tieshan magnetite contain a FeO (total) content of 85.980–93.185 wt% (average 91.231 wt%) and 88.412–92.089 wt% (average 89.299 wt%), respectively. The Longqiao magnetite contains high SiO_2 (< 0.011–2.384 wt%, average: 0.210 wt%), Al_2O_3 (0.039–2.375 wt%, average: 0.498 wt%), MgO (< 0.006–1.271 wt%, average: 0.142 wt%) and MnO (< 0.018–1.171 wt%, average: 0.222 wt%) and low TiO_2 (< 0.014–0.687 wt%, average: 0.209 wt%), CaO (< 0.008–0.679 wt%, average: 0.177 wt%) and Cr_2O_3 (< 0.012–0.159 wt%, average: 0.084 wt%) (Table 1). The contents of NiO and V_2O_3 are mostly below

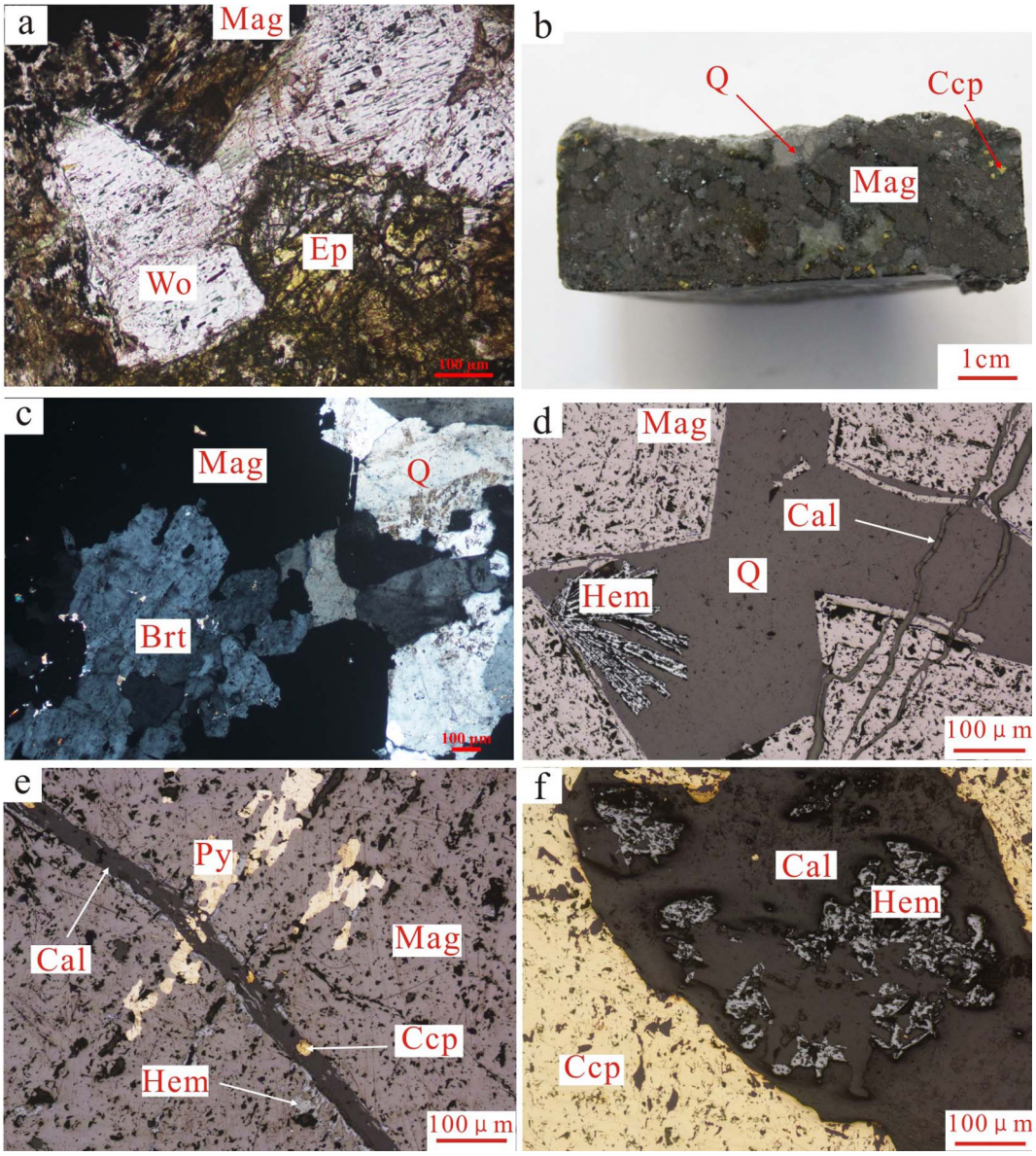

Fig. 5. Photomicrographs of iron ores from the Longqiao Fe deposit. (a) Epidote replaced wollastonite, and is replaced by magnetite (plane-polarized light); (b) Massive ore, mainly contains magnetite and little quartz and chalcopyrite; (c) Magnetite crosscut barite, and associate with quartz (cross-polarized light); (d) Magnetite closely associated with quartz and hematite, and calcite veins crosscut magnetite and quartz (reflected light); (e) Sulfides and calcite veins crosscut magnetite of the magnetite stage (reflected light); (f) Chalcopyrite associated with calcite and hematite (reflected light). Mineral abbreviations: *Mag*: magnetite, Wo: wollastonite, *Ep: epidote, Sid*: siderite, *Q*: quartz, Brt: barite, *Hem*: hematite, *Cal*: Calcite, *Py*: Pyrite, *Ccp*: Chalcopyrite.

the detection limits. The Tieshan magnetite contains high MgO (0.023–2.148 wt%, average: 0.897 wt%), SiO_2 (0.016–0.972 wt%, average: 0.416 wt%) and Al_2O_3 (0.122–0.528 wt%, average: 0.286 wt%) and low CaO (< 0.008–0.469 wt%, average: 0.173 wt%), MnO (< 0.018–0.185 wt%, average: 0.094 wt%), Cr_2O_3 (0.015–0.082 wt%, average: 0.045 wt%) and V_2O_3 (< 0.011–0.031 wt%, average: 0.019 wt%) (Table 1). The contents of NiO and TiO_2 are mostly below the detection limits.

Results show that the Longqiao and Tieshan magnetite contains a weak negative correlation between the FeO(total) content and SiO_2, Al_2O_3, MgO and MnO contents, which may indicate that these elements were incorporated into the intracrystalline sites of magnetite by substitution of Si^{4+}, Al^{3+}, Mg^{2+} and Mn^{2+} for Fe^{2+} and/or Fe^{3+} (Fig. 8). Besides, the Longqiao magnetite contents display slightly higher average Al_2O_3, MnO and lower average SiO_2 and MgO concentrations than the Tieshan magnetite (Fig. 8).

4.2.2. LA-ICP-MS

The mean contents of trace elements determined by LA-ICP-MS and standard deviation of the selected elements for each sample of the Longqiao and Tieshan magnetite are summarized in Table 2 and detailed results are given in the Appendix A.

As illustrated in Fig. 9, trace element contents in magnetite from the Longqiao deposit vary by less than one order magnitude, whereas those from the Tieshan deposit vary by less than two orders of magnitude. Magnetites from the Longqiao deposit have higher Al, Ti, V, Ni, Ga and Sn contents, whereas magnetites from the Tieshan deposit have higher Mg and Co contents. The Longqiao and Tieshan deposits have similar contents of Ca, Cr, Mn and Zn. Compositional variations between magnetite samples from the Longqiao and Tieshan deposits can be further identified by binary plots of selected elements (Fig. 10). In these plots, magnetite trace elements define two separated fields for the Longqiao and Tieshan deposits. Gallium shows a weakly negative correlation with Sn for both the Longqiao and Tieshan deposits. There is a

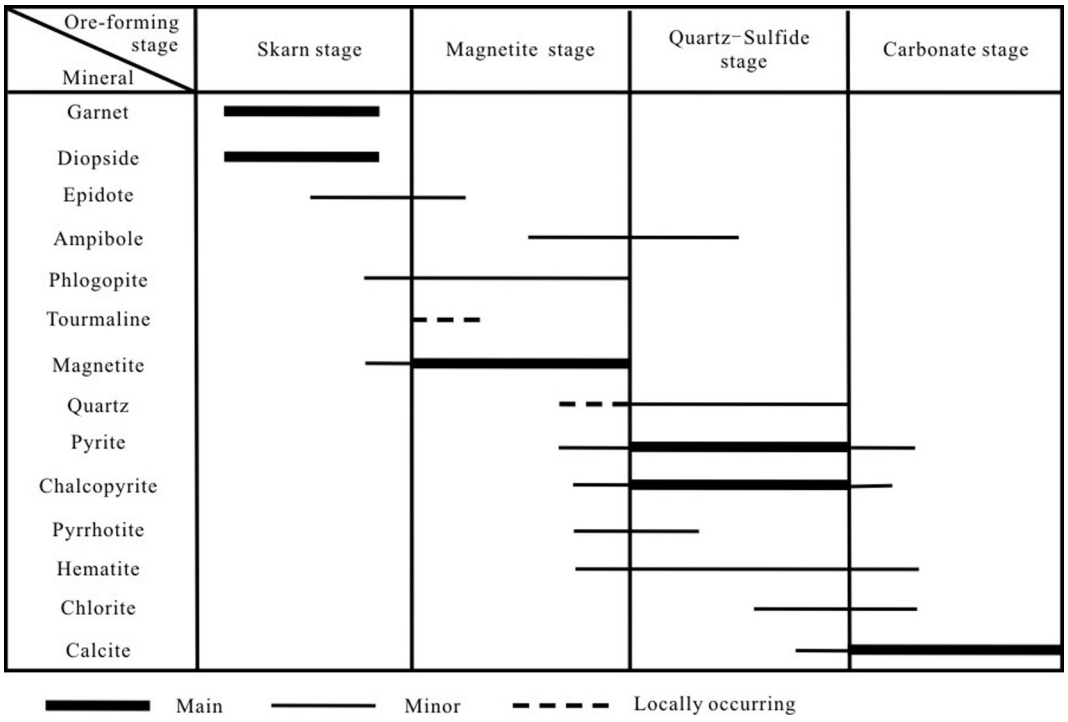

Fig. 6. Mineralization paragenesis of the Tieshan Fe–Cu deposit.

strong positive correlation between Ni and Cr, Ga and Al, V and Ti for the Tieshan deposit, whereas Ni and Al, Al and Mg show a weakly positive correlation. In addition, Ga and Al, V and Ti, Al and Mg also show a positive correlation for the Longqiao deposit, whereas there is no obvious correlation between Ni and Cr or Ni and Al (Fig. 10).

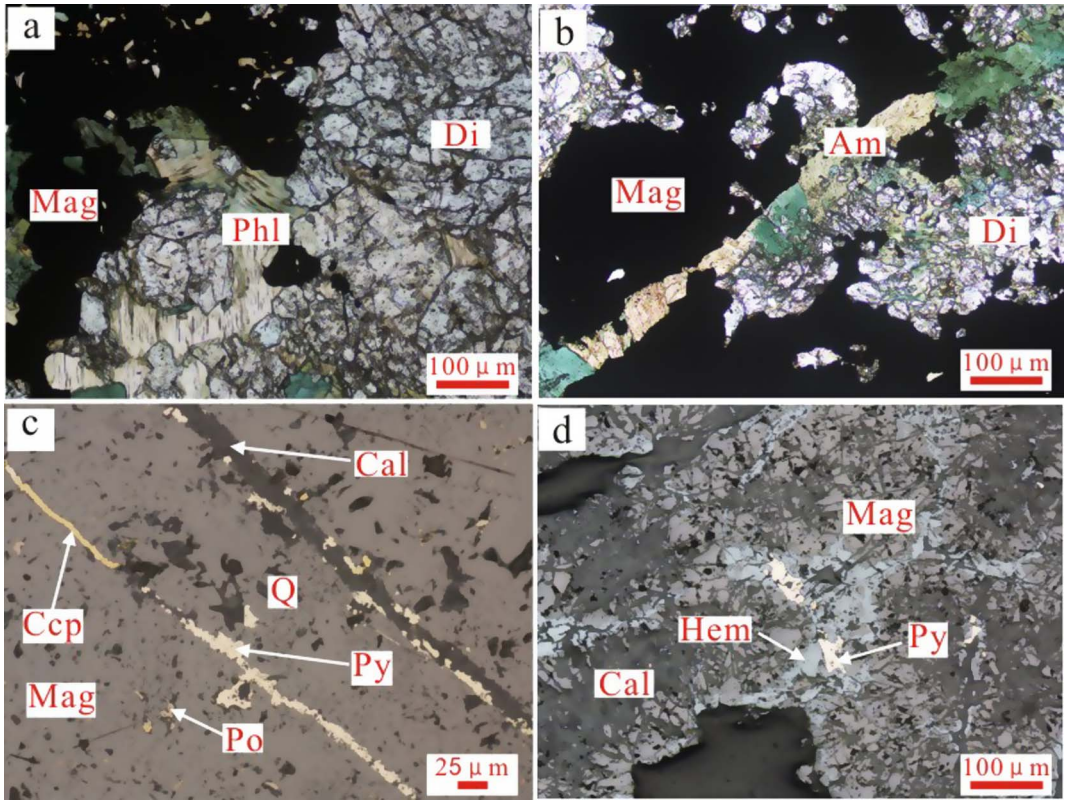

Fig. 7. Photomicrographs of iron ores from the Tieshan Fe–Cu deposit. (a). Phlogopite replaced diopside along the margin or fractures, and is replaced by magnetite (plane-polarized light); (b). Amphibole veins crosscut magnetite and diopside (plane-polarized light); (c). Quartz closely associated with sulfides, and pyrite and chalcopyrite veins crosscut magnetite of the magnetite stage (reflected light); (d). Magnetite crosscut by post-mineralized calcite veins, and replaced by hematite along fissures (reflected light). Mineral abbreviations: *Mag*: magnetite, *Q*: quartz, *Hem*: hematite, *Cal*: Calcite, *Py*: Pyrite, *Ccp*: Chalcopyrite, *Phl*: phlogopite, *Di*: diopside, *Am*: amphibole, *Po*: pyrrhotite.

Table 1
Electron microprobe analyses (wt%) of representative magnetite from the Longqiao and Tieshan deposits.

Sample	SiO_2	Al_2O_3	MgO	CaO	TFeO	MnO	Cr_2O_3	V_2O_3	TiO_2	NiO	Total
D.L.	0.011	0.008	0.006	0.019	0.018	0.018	0.012	0.011	0.014	0.016	
LQ-2-1	1.387	1.643	1.271	0.233	85.980	1.171	0.013	0.071	0.199	b.d.	91.975
LQ-2-2	1.175	2.375	1.103	0.251	86.231	1.040	b.d.	0.036	0.062	b.d.	92.276
LQ-2-3	1.648	2.155	1.161	0.397	86.693	0.798	0.035	0.041	0.038	b.d.	92.966
LQ-2-4	0.650	1.433	1.180	b.d.	88.003	1.020	0.064	0.044	0.047	b.d.	92.641
LQ-4-1	0.055	0.039	0.003	b.d.	92.607	0.130	0.081	0.030	0.034	b.d.	92.982
LQ-4-2	1.487	0.332	0.252	0.303	91.280	0.102	0.127	0.023	b.d.	0.041	92.947
LQ-4-3	2.384	0.683	0.382	0.679	89.709	0.182	0.070	0.038	0.080	b.d.	92.208
LQ-5-1	b.d.	0.532	0.031	b.d.	92.508	0.068	0.098	b.d.	0.121	0.022	93.389
LQ-5-2	0.017	0.335	0.009	0.340	92.986	0.036	0.035	0.018	0.073	b.d.	93.509
LQ-5-3	0.052	0.415	0.027	0.240	91.888	0.057	0.043	b.d.	0.113	b.d.	92.595
LQ-5-4	0.027	0.295	0.008	0.361	92.610	0.068	0.073	b.d.	0.098	b.d.	93.183
LQ-5-5	0.069	0.304	0.052	0.340	93.185	0.133	0.068	b.d.	0.081	b.d.	93.907
LQ-5-6	0.020	0.399	b.d.	0.231	92.243	0.074	0.101	b.d.	0.089	b.d.	92.930
LQ-5-7	0.050	0.353	b.d.	0.320	87.866	0.073	0.049	b.d.	0.090	b.d.	88.485
LQ-5-8	0.040	0.385	0.058	b.d.	91.853	0.113	0.068	b.d.	0.068	b.d.	92.585
LQ-6-1	0.021	0.510	0.021	b.d.	91.678	0.286	0.100	b.d.	0.549	b.d.	93.165
LQ-6-2	0.015	0.407	0.022	0.341	91.081	0.281	0.112	b.d.	0.570	b.d.	92.488
LQ-6-3	0.033	0.450	0.050	0.343	90.642	0.327	0.159	b.d.	0.687	b.d.	92.348
LQ-6-4	0.014	0.291	0.074	0.330	92.275	0.089	0.085	b.d.	0.114	b.d.	92.952
LQ-6-5	0.020	0.529	0.051	0.220	91.439	0.223	0.088	b.d.	0.316	b.d.	92.666
LQ-6-6	0.049	0.411	0.048	0.290	91.223	0.175	0.094	b.d.	0.254	b.d.	92.254
LQ-6-7	0.030	0.532	0.055	b.d.	90.729	0.286	0.097	b.d.	0.445	b.d.	92.174
LQ-6-8	0.036	0.266	0.064	b.d.	92.061	0.195	0.088	b.d.	0.232	b.d.	92.942
LQ-6-9	0.041	0.199	0.023	0.290	91.993	0.036	0.100	0.021	0.023	b.d.	92.438
LQ-6-10	0.034	0.481	0.015	b.d.	91.366	0.375	0.091	b.d.	0.601	b.d.	92.968
LQ-6-11	0.019	0.467	0.017	b.d.	91.048	0.354	0.091	b.d.	0.631	b.d.	92.627
LQ-6-11-1	0.022	0.203	0.032	b.d.	91.821	0.105	0.076	0.022	0.164	b.d.	92.456
LQ-6-12	0.034	0.201	0.024	b.d.	92.092	0.120	0.103	b.d.	0.151	b.d.	92.730
LQ-6-13	b.d.	0.194	0.012	b.d.	91.521	0.084	0.106	b.d.	0.052	b.d.	91.977
LQ-7-1	b.d.	0.225	0.045	b.d.	92.522	0.130	0.101	0.012	0.062	b.d.	93.101
LQ-7-2	0.028	0.157	0.013	0.320	92.020	0.010	0.058	b.d.	0.032	b.d.	92.318
LQ-7-3	0.024	0.173	0.027	0.263	91.984	0.059	0.087	b.d.	0.022	b.d.	92.389
LQ-7-4	0.033	0.469	0.045	b.d.	91.186	0.106	0.073	b.d.	0.038	b.d.	91.950
LQ-7-5	0.016	0.106	0.007	0.284	91.869	0.041	0.062	b.d.	0.103	b.d.	92.214
LQ-7-6	0.023	0.491	0.070	0.283	91.617	0.143	0.108	b.d.	0.056	b.d.	92.508
LQ-7-7	0.021	0.459	0.015	b.d.	91.912	0.088	0.088	b.d.	0.066	b.d.	92.660
LQ-7-8	0.022	0.354	0.031	0.261	91.890	0.088	0.093	b.d.	0.110	b.d.	92.596
LQ-7-9	0.033	0.616	0.178	0.284	91.888	0.153	0.074	b.d.	0.121	b.d.	93.063
LQ-8-1	0.032	0.498	0.053	b.d.	91.325	0.241	0.064	b.d.	0.479	b.d.	92.692
LQ-8-2	0.038	0.316	0.010	0.287	91.641	0.174	0.102	b.d.	0.314	0.020	92.615
LQ-8-3	0.018	0.366	0.026	0.301	91.244	0.155	0.114	b.d.	0.382	b.d.	92.305
LQ-8-4	0.025	0.334	0.008	b.d.	91.659	0.109	0.122	b.d.	0.330	b.d.	92.587
LQ-8-5	0.021	0.342	0.016	b.d.	92.072	0.145	0.086	0.022	0.210	b.d.	92.914
LQ-8-6	0.030	0.413	0.017	b.d.	91.479	0.104	0.097	b.d.	0.242	b.d.	92.384
LQ-8-7	0.048	0.521	0.030	0.220	91.185	0.354	0.083	b.d.	0.632	b.d.	92.853
LQ-8-8	0.011	0.306	0.024	0.324	92.415	0.193	0.111	b.d.	0.285	b.d.	93.355
LQ-8-9	0.026	0.450	0.024	b.d.	91.353	0.133	0.096	b.d.	0.338	b.d.	92.426
TS-78-2-1	0.139	0.186	0.023	b.d.	88.589	b.d.	0.058	0.016	b.d.	b.d.	89.011
TS-78-2-2	0.056	0.156	0.032	b.d.	89.032	b.d.	0.082	0.015	b.d.	b.d.	89.377
TS-122-1	0.067	0.122	0.024	b.d.	89.228	b.d.	0.019	0.022	b.d.	b.d.	89.491
TS-122-2	0.016	0.189	0.033	b.d.	88.471	b.d.	0.055	0.022	b.d.	b.d.	88.789
TS-136-1	0.021	0.234	0.474	b.d.	92.089	0.095	0.019	0.031	b.d.	b.d.	92.970
TS-136-2	0.862	0.528	0.337	0.408	89.257	0.134	0.043	0.020	b.d.	0.030	92.621
TS-150-1-1	0.534	0.312	1.475	b.d.	89.519	0.185	0.067	0.029	b.d.	b.d.	92.121
TS-150-1-2	0.682	0.324	1.600	0.096	90.088	0.164	0.051	0.012	b.d.	b.d.	93.017
TS-200-1	0.972	0.275	1.738	0.463	89.149	0.140	0.069	0.030	b.d.	b.d.	92.836
TS-200-2	0.675	0.358	1.981	0.469	88.412	0.171	0.017	0.016	b.d.	b.d.	92.323
TS-200-3	0.556	0.467	2.148	0.462	88.452	0.148	0.015	b.d.	b.d.	b.d.	92.263

Abbreviations: D.L. = detection limits; b.d. = below detection.

5. Discussion

5.1. Factors controlling magnetite compositions

The geochemical composition of magnetite deposited from hydrothermal fluids may be mostly controlled by a number of factors: (1) composition of ore fluids, (2) composition of host rocks that have reacted with the fluids, (3) nature of co-crystallizing minerals, and/or (4) physicochemical conditions (e.g., temperature (T) and oxygen fugacity (fO_2)) during mineral formation (Nystroem and Henriquez, 1994; Toplis and Corgne, 2002; Carew, 2004; Dare et al., 2014; Dupuis and Beaudoin, 2011; Nadoll et al., 2014a,b, 2012). Therefore, in order to constrain the nature and origin of the ore-forming fluids using magnetite compositions, the first step is to understand whether, and to what extent, these controls affect trace element compositions of magnetite from these deposits.

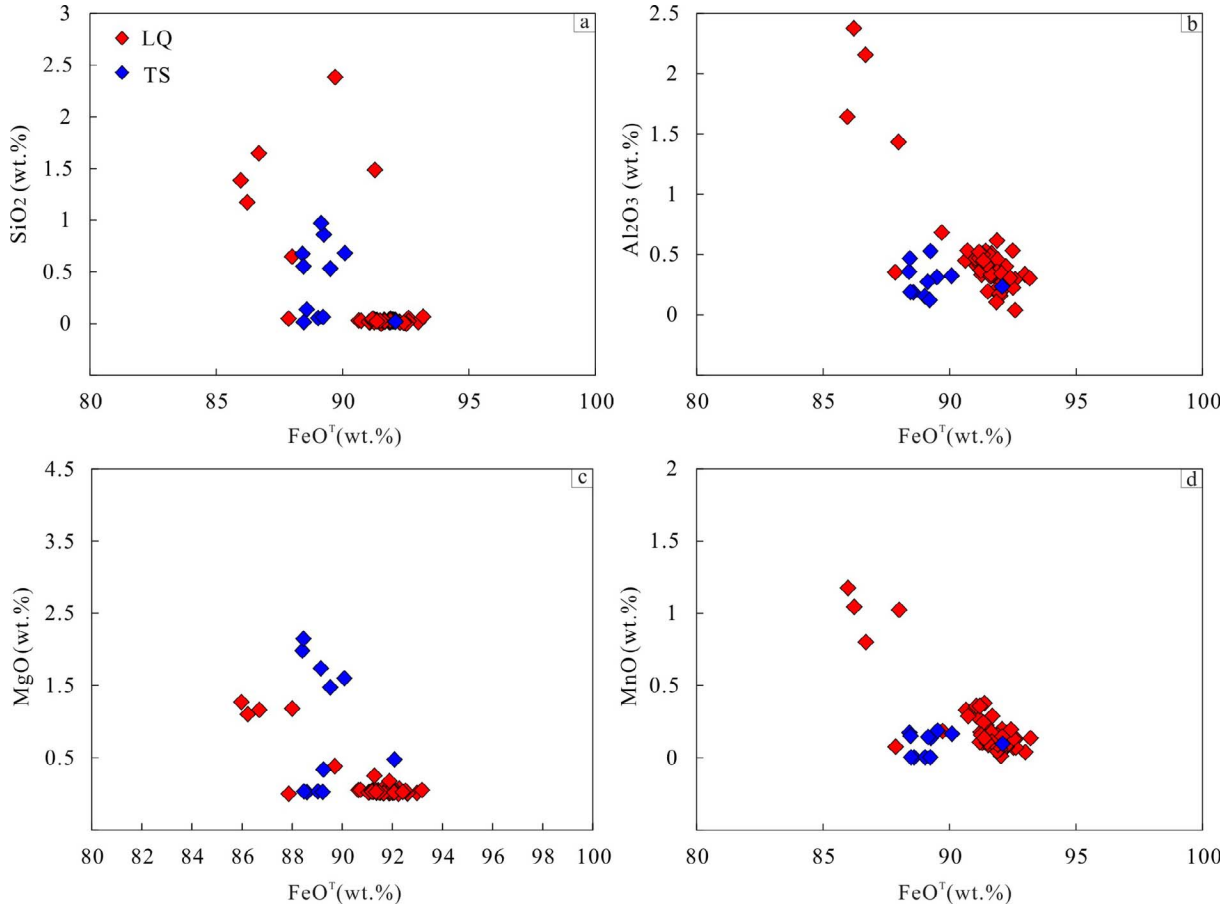

Fig. 8. Scatter plots of the Longqiao (LQ) and Tieshan (TS) magnetite. (a) SiO_2 vs. FeO^T; (b) Al_2O_3 vs. FeO^T; (c) MgO vs. FeO^T; (d) MnO vs. FeO^T.

Table 2
LA-ICP-MS results (in parts per million) of representative magnetite from the Longqiao and Tieshan deposits.

		Mg	Al	Ca	Ti	V	Cr	Mn	Co	Ni	Zn	Ga	Sn
D.L.		0.01	0.18	172.53	0.27	0.06	0.85	0.28	0.02	0.28	0.40	0.04	0.07
LQ-2	ave (n = 4)	5016.38	8821.97	3108.81	1073.19	209.89	11.45	3728.92	53.78	0.28	0.40	0.04	0.07
	stdev	807.97	850.15	246.24	113.23	22.23	7.78	1739.83	11.51	8.49	387.99	30.53	15.26
LQ-8	ave (n = 10)	4187.55	6837.93	3626.34	1309.44	211.09	13.78	1884.35	54.24	0.75	218.60	1.10	5.66
	stdev	900.52	1747.85	884.81	199.57	8.69	3.89	265.57	9.09	8.57	183.30	19.82	17.15
LQ-7	ave (n = 9)	4377.67	7462.64	3153.57	1296.02	211.36	12.01	2889.27	53.66	1.28	36.36	6.04	3.59
	stdev	868.38	1458.96	639.76	311.56	41.72	3.61	1008.88	6.34	7.85	304.02	26.23	16.72
LQ-6	ave (n = 9)	4765.79	6032.85	3248.45	1139.56	205.54	11.06	4963.12	54.23	0.96	63.24	5.09	4.00
	stdev	955.68	472.57	613.74	233.05	31.51	4.03	2220.13	5.44	8.18	354.48	27.68	16.30
LQ-5	ave (n = 6)	4829.06	7306.51	3035.63	1261.50	246.60	11.53	3309.55	53.83	0.85	143.60	1.56	3.75
	stdev	1116.11	1420.66	557.40	239.27	26.35	3.11	1251.89	5.26	9.04	390.27	26.82	16.05
TS-78-2	ave (n = 2)	6633.92	3946.38	3661.93	169.11	46.19	28.94	992.47	44.21	1.08	158.38	2.90	3.70
	stdev	53.77	793.78	52.07	12.87	5.60	8.26	4.83	26.57	5.42	103.41	7.35	3.04
TS-122	ave (n = 3)	8879.33	5331.85	2909.24	422.96	146.20	7.55	2240.02	110.19	0.04	21.71	0.18	0.02
	stdev	173.61	275.04	409.31	26.42	14.01	2.40	157.94	63.14	3.55	246.00	11.74	2.43
TS-136	ave (n = 4)	10230.37	3832.63	4071.85	440.35	184.75	15.49	1751.40	81.19	0.23	58.96	0.46	0.27
	stdev	3562.96	1341.92	407.91	59.27	5.41	14.97	104.29	47.68	2.57	217.31	11.48	5.87
TS-150-1	ave (n = 3)	10356.56	2002.66	2947.45	193.51	160.94	3.95	2530.56	90.55	2.06	72.07	1.91	1.71
	stdev	1129.88	217.63	481.17	20.26	15.54	2.15	19.93	3.38	0.98	269.64	5.68	5.47
TS-200	ave (n = 2)	10492.11	2070.79	3694.48	195.44	67.62	19.17	2046.10	80.77	0.21	34.11	0.34	0.71
	stdev	67.08	287.50	306.35	2.75	5.61	0.79	96.59	82.71	5.16	230.38	10.73	4.96

Abbreviation: D.L. = detection limit; ave = average; stdev = standard deviation; n = the number of analyzed spots.
Detection limit (D.L.) = $3 \times \sigma^i_{background} \times C^i_{RM}/cps^i_{RM}$, where $\sigma^i_{background}$ is the standard deviation of multiple determinations of element i in the background, C^i_{RM} and cps^i_{RM} are concentration and peak intensity of element i in the reference material, respectively.

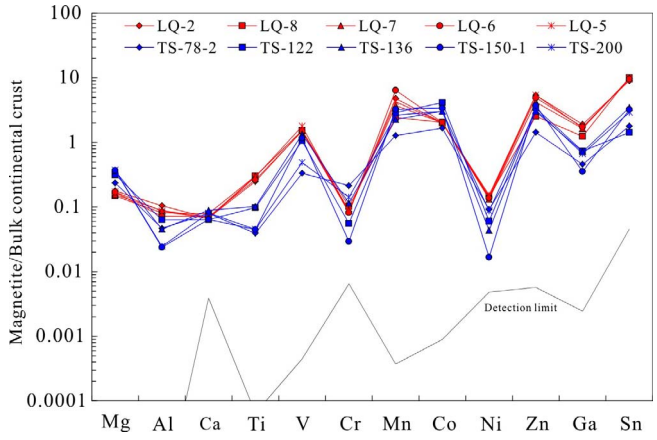

Fig. 9. Multi-element variation diagram of the average trace element concentrations in magnetite normalized to bulk continental crust (Rudnick and Gao, 2003).

5.1.1. *Fluid-rock interaction*

Fluid-rock interaction and primary mineral replacement can provide hydrothermal magnetite with some geochemical features of the altered host rocks or minerals (Carew, 2004; Nadoll et al., 2014a). In skarn systems, fluid-rock interaction or host rock buffering are considered to be the major control of magnetite geochemistry (Nadoll et al., 2014a,b). It has been shown that elements such as Mg and Mn can successively be enriched in hydrothermal fluids by extensive fluid-rock interaction (Einaudi et al., 1981; Meinert, 1992). Magmatic fluids are generally enriched in Si, Al, Na, K, Fe, F, and Cl (Tosdal et al., 2009) and carbonates are enriched in Ca, Mg, and Mn. These elements have similar element partitioning behaviors during magnetite crystallization, and thus the (Mg + Mn) vs. (Si + Al)/(Mg + Mn) diagram can reflect the degree of fluid-rock interactions (Hu et al., 2014a,b).

The decreasing (Si + Al)/(Mg + Mn) and increasing (Mg + Mn) of magnetite indicate decreasing magmatic fluid/carbonate rock ratios (Hu et al., 2014a,b). The Tieshan magnetite from the main

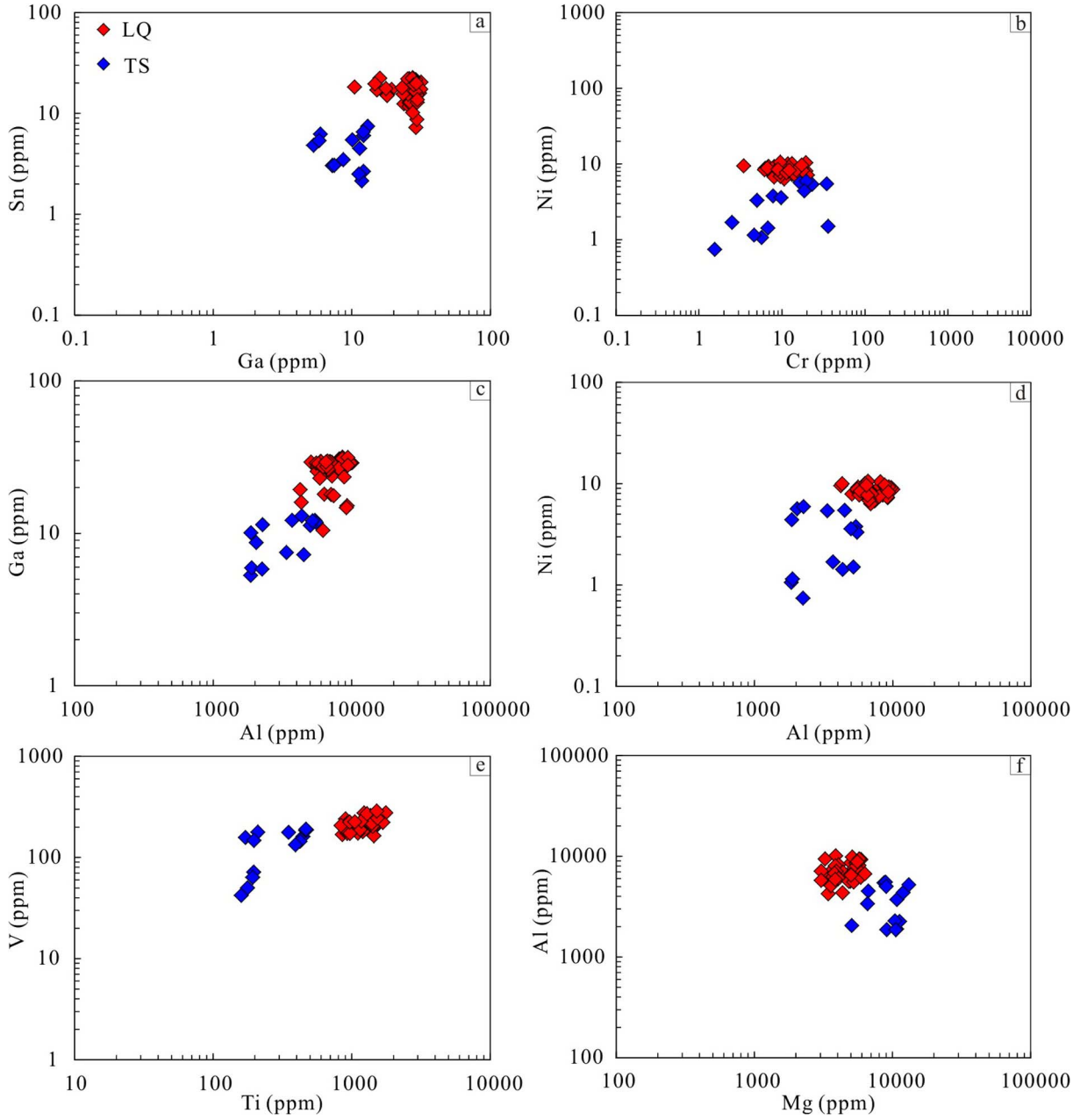

Fig. 10. Binary plots of selected trace elements in magnetite from the Longqiao and Tieshan deposit.

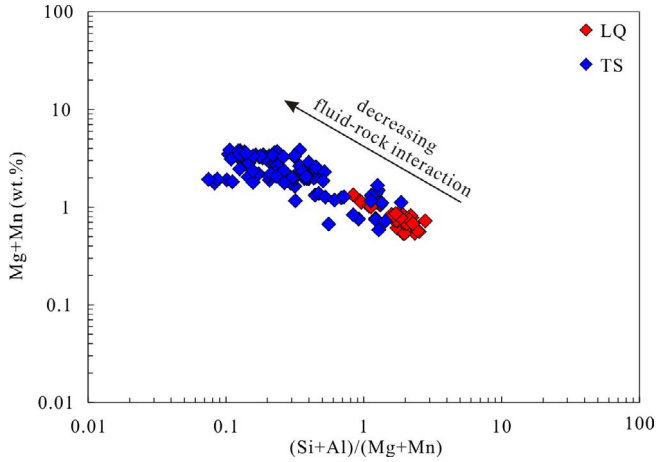

Fig. 11. Plot of (Mg + Mn) vs. (Si + Al)/(Mg + Mn) for the Longqiao (LQ) and Tieshan (TS) magnetite. Part of the Tieshan magnetite data are from Wang et al., 2016.

mineralization stage contains slightly higher average (Mg + Mn) contents but lower (Si + Al)/(Mg + Mn) values than the Longqiao magnetite, indicating a lower degree of fluid–rock interactions at Tieshan (Fig. 11). The more variable Mg + Mn content and (Si + Al)/(Mg + Mn) values for the Tieshan magnetite compared with the Longqiao magnetite may indicate that fluid-rock interaction was more variable and at least locally more dominant at Tieshan (Fig. 11).

As illustrated in the scatter plots (Fig. 8), magnetite composition of the Longqiao Fe deposit is quite different from that of the Tieshan Fe–Cu deposit. The Longqiao magnetite contents display slightly higher average Al_2O_3 and MnO, and lower average SiO_2 and MgO concentrations than the Tieshan magnetite. The Longqiao orebodies are mainly hosted by dolomite, limestone and pelitic siltstone of the Dongma'anshan Formation, while the Tieshan deposit is related to the Early Cretaceous Tieshan intrusive complex that intruded the Daye Formation marine carbonates, withthe orebodies located predominantly along the marble–quartz diorite contact. Therefore, the differences between magnetite chemistry may be caused by different host rock compositions of the Longqiao and Tieshan deposits.

5.1.2. Co-crystallizing minerals

Minerals co-crystallizing with magnetite may affect the trace element concentrations within the magnetite due to different partition coefficients between them (Dare et al., 2014; Nadoll et al., 2014a). For example, chalcophile elements may be partitioned preferentially into sulfides compared to magnetite (Dare et al., 2014). In magmatic Fe–Ti–V deposits, minerals co-crystallizing with magnetite, such as olivine, pyroxenes, plagioclase and apatite, have little influence on the magnetite trace element contents because most elements (REE, P, Li, Sc, Sr, Ba, U, Th) compatible in these silicates/phosphates are incompatible in magnetite (Liu et al., 2015). On the other hand, concentrations of Co, Ni, Mo, Sn, Zn and Pb in magnetite would be affected by sulfides because these elements can partition into both magnetite and sulfide phases in sulfide-bearing magmatic and hydrothermal systems (e.g., Nadoll et al., 2014a; Chen et al., 2015a; Huang et al., 2016).

The normalized multi-element variation diagrams of the Longqiao and Tieshan deposits show that the Longqiao magnetites have higher Ti, V, Ni, Ga and Sn contents and lower Co content (Fig. 9). And the binary plots of trace element concentrations in magnetite from these deposits also plotted in different fields (Fig. 10). Therefore, these elements can be used to differentiate the Longqiao and Tieshan deposits. According to the paragenesis and mineralization stages described in the previous section, Longqiao magnetites from the main mineralization stage are intergrown with quartz and replace epidote and barite (Fig. 5), and are characterized by the mineral assemblage of magnetite – quartz ± hematite ± tourmaline (Fig. 4). Tieshan magnetites are intergrown with phlogopite and replaced diopside from the skarn alteration stage, with a mineral assemblage of magnetite – phlogopite (Fig. 6). The different mineral assemblages of magnetite mineralization may help explain the variable contents of trace elements of magnetite from the Longqiao and Tieshan deposits. For example, lower Ti, V, Ni, Ga and Sn contents of Tieshan magnetites may result from its coexistence with phlogopite and the preferential partitioning of these elements in phlogopite. However, higher Co content in Tieshan magnetites are likely the result of additional factors (e.g., the composition of host rocks, temperature and fO_2).

5.1.3. Temperature and fO_2

Temperature is considered to be another major geochemical controlling factor for hydrothermal magnetite since element partition coefficients are greatly temperature dependent (McIntire, 1963). High-temperature porphyry and skarn magnetite shows relatively high trace element concentrations, whereas un-metamorphosed magnetite from banded iron formation (BIF) has the lowest trace element concentrations (Nadoll et al., 2014a). Titanium in Fe oxides is regarded to be positively correlated with temperature (Nadoll et al., 2012; Dare et al., 2012). Consequently, in the (Al + Mn) vs. (Ti + V) diagram (Fig. 12a), higher (Al + Mn) and (Ti + V) contents of the Longqiao magnetite may suggest higher ore-forming temperature than the Tieshan deposit.

Some elements, such as vanadium, can occur in various valence states and therefore their behaviors are strongly fO_2-linked (Nielsen et al., 1994; Righter et al., 2006). The oxidation state of V in natural environments varies from +3 to +5, but the +3 state is only found in extremely reduced systems (e.g., Takeno, 2005), whereas the common

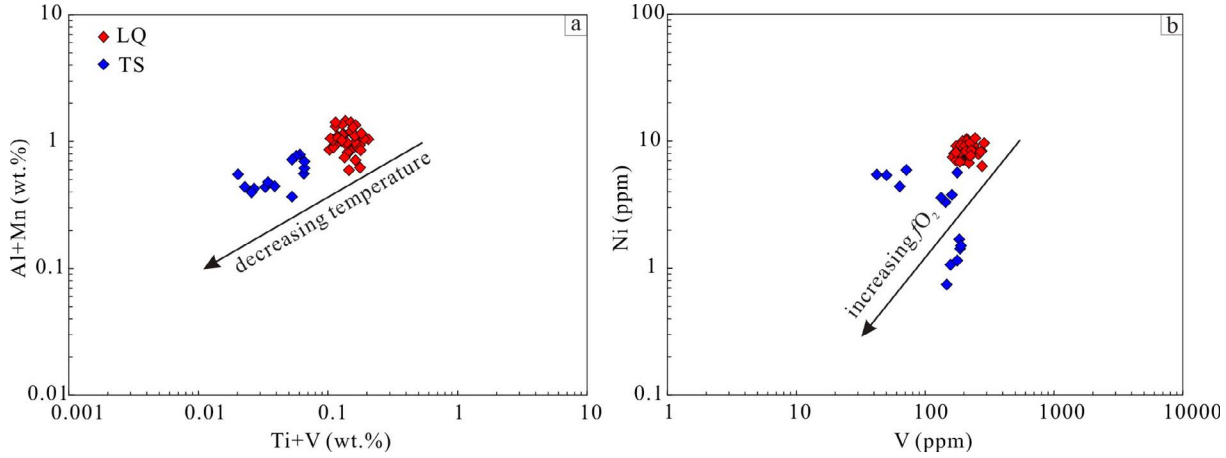

Fig. 12. Plots of (a) (Al + Mn) vs. (Ti + V) and (b) Ni vs. V for the Longqiao and Tieshan magnetite. (Fig. 12a modified from Nadoll et al., 2014a).

fugacity range permits the occurrence of V^{3+}, V^{4+}, and V^{5+}. Among these species, V^{3+} has the highest compatibility with the spinel structure of magnetite (e.g., Balan et al., 2006; Righter et al., 2006). In silicate melt experiments, the fractionation of V into magnetite is a function of fO_2 (Toplis and Corgne, 2002; Righter et al., 2006). The magnetite/liquid partition coefficient for V decreases with increasing fO_2, as V^{3+} is less stable under these conditions. Phase diagrams of V aqueous species also show a predominance of V^{3+} in reducing environments (Takeno, 2005), and that even a small increase in fO_2 could convert it to V^{4+}, which is less compatible within the magnetite structure. Longqiao magnetites have higher average V contents (205.54 – 246.60 ppm) than Tieshan magnetites (46.19 – 184.75 ppm), which indicates that the ore fluids at Longqiao were likely more reduced than those at Tieshan (Table 2, Fig. 12b).

5.2. Implications for deposit types and ore genesis

The Longqiao Fe deposit was first considered as an exhalative sedimentary deposit (Ren et al., 1991), but was later interpreted by Ni et al. (1994) to be a sedimentary deposit with a hydrothermal overprint. However, more recently, Zhou et al. (2011) considered that the Longqiao deposit is a skarn-type stratabound mineral system. Therefore, the debate is centralized on the derivation of the ore-forming fluids from sedimentary strata, magmatic hydrothermal process, or both. The Tieshan Fe–(Cu) deposit was first considered to be a magmatic deposit (Zhai et al., 1982). However, several studies argue that the deposit is a skarn or a product of hydrothermal metasomatism rather than related to magmatic processes (Zhao, 1990; Duan et al., 2014; Hu et al., 2015; Wang et al., 2015).

The element composition of magnetite varies greatly between different ore-forming environments, therefore, a number of discrimination diagrams were proposed to discriminate magnetite from different deposit types or different metallogenic environments (Chen et al., 1987; Dare et al., 2014; Dupuis and Beaudoin, 2011; Lin, 1982; Nadoll et al., 2014a,b).

In the TiO_2–Al_2O_3–(MgO + MnO) ternary diagram that was originally proposed by Lin (1982), most of the Longqiao magnetite fall into the contact metasomatic and skarn field and some into the metasedimentary field, which suggests that the Longqiao magnetite has both hydrothermal and sedimentary affinities. Almost all the data presented here for magnetite from the Tieshan deposit fall into the skarn field, suggesting that the Tieshan Fe–(Cu) deposit is a hydrothermal deposit (Fig. 13a).

In the (Ca + Al + Mn) vs. (Ti + V) magnetite discrimination diagram (Dupuis and Beaudoin, 2011), the Longqiao and Tieshan magnetite fall into the skarn field (Fig. 13b), suggesting a hydrothermal metasomatic origin. By comparing these two deposits with the Fenghuangshan skarn-type deposit and Washan porphyry-type deposit in the MLYRB, we discover that both Longqiao and Tieshan deposits are quite different from the Washan porphyry-type deposit (most fall into the Fe–Ti, V field and some into the porphyry field) and the characteristics of the Tieshan deposit are very similar to the Fenghuangshan skarn deposit, whereas the Longqiao deposit shows differences from the Fenghuangshan skarn deposit (Fig. 13b).

The orebodies and ores of the Longqiao Fe deposit display sedimentary features, for example, orebodies occur as stratified beds in the carbonate rocks of the Middle Triassic Dongma'anshan Formation. Limestone from the Dongma'anshan Formation and the Longqiao Fe deposit have a carbon and oxygen isotope composition similar to that of marine sedimentary carbonates (Zhou et al., 2011). Some ores exhibit laminated to banded structures, whereas some minerals (e.g., barite) that are coeval with sedimentary ore minerals are replaced by magnetite, which indicates that the Longqiao deposit may have been partially formed by hydrothermal superimposition and transformation of the early sediments (Fig. 5c). Moreover, our new magnetite geochemical data suggest that the Longqiao magnetite are distinguished from a typical skarn origin in that they record a combination of hydrothermal metasomatism with a minor influence from that sedimentary host rocks (Fig. 13a).

The Tieshan Fe–(Cu) deposit is widely accepted to be skarn-type (Zhao, 1990; Duan et al., 2014; Wang et al., 2015, 2016), although an earlier study had also suggested formation by injected Fe-rich magma (Zhai et al., 1982). The Tieshan Fe–(Cu) deposit is related to the Early Cretaceous Tieshan intrusive complex that intruded the Daye Formation marine carbonates. The stratiform/lensoidal orebodies are hosted in the Daye Formation marble. Our magnetite geochemical data show that Tieshan is a typical skarn deposit and may have formed via hydrothermal metasomatism (Fig. 13).

6. Conclusions

Magnetites from the Longqiao and Tieshan deposits have different geochemistry, and can be clearly discriminated by the Sn vs. Ga, Ni vs. Cr, Ga vs. Al, Ni vs. Al, V vs. Ti, and Al vs. Mg diagrams. Such differences may be applied to distinguish other typical skarn (Tieshan) and multi-origin hydrothermal (Longqiao) deposits in the MLYRB. The

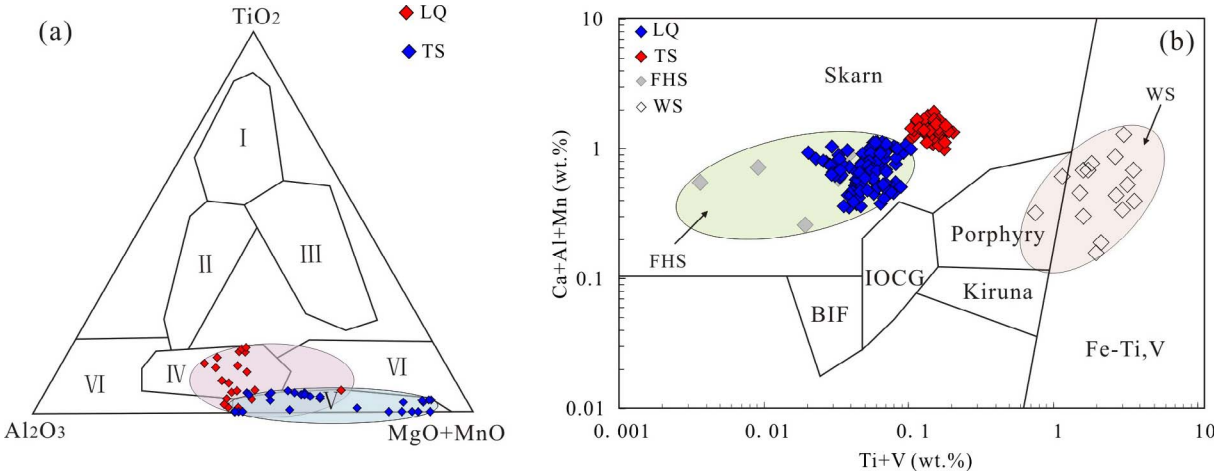

Fig. 13. (a) Ternary TiO_2–Al_2O_3–(MgO + MnO) plot for the Longqiao and Tieshan magnetite. The reference fields are from Lin, 1982. I = accessory mineral type; II = magmatic type; III = volcanic type; IV = contact metasomatic type; V = skarn type; VI = metasedimentary type. (b) (Ca + Al + Mn) vs. (Ti + V) genetic classification diagram of the Longqiao and Tieshan magnetite. The reference fields are from Dupuis and Beaudoin, 2011. BIF = banded iron formation, Skarn = Fe–Cu skarn deposits, IOCG = iron oxide–copper–gold deposits, Porphyry = porphyry Cu deposits, Kiruna = Kiruna apatite–magnetite deposits, Fe–Ti, V = magmatic Fe–Ti–V–oxide deposits. Part of the Tieshan magnetite data are from Wang et al., 2016. Data of the Fenghuangshan (FHS) Cu–Fe–Au skarn deposit and Washan (WS) porphyrite-type Fe deposit are from Huang et al. (2016) and Duan et al. (2012), respectively.

fluid–rock interactions, influence of the co-crystallizing minerals and other physicochemical parameters, such as temperature and fO_2, may have together controlled the magnetite trace element contents of both deposits. The Tieshan deposit may have had higher degree of fO_2, but lower fluid–rock interactions and magnetite forming temperature than the Longqiao deposit.

The TiO_2–Al_2O_3–(MgO + MnO) and (Ca + Al + Mn) vs. (Ti + V) magnetite discrimination diagrams show that the Longqiao magnetite is characteristic of both sedimentary and hydrothermal origin, whereas the Tieshan magnetite is characteristic of hydrothermal metasomatic origin typical of skarn deposits. This result is consistent with the ore characteristics that the Longqiao contains two types of ores (lamellar and massive ores), whereas the Tieshan only contains massive ores.

Acknowledgements

This study was funded by the National Natural Science Foundation of China (41572059), Creative and Interdisciplinary Program, CAS (Y433131A07) and SKL-ODG Open Funds (201508). We thank Dr. Congying Li (Guangzhou Institute of Geochemistry, Chinese Academy of Sciences) for the EMPA and LA-ICP-MS assistance. We are also grateful to Profs. Taofa Zhou and Jianwei Li for supplying some of the Longqiao and Tieshan ore samples.

Appendix A. Supplementary data

Supplementary data for the LA-ICP-MS analysis (in parts per millions) of representative magnetite from the Longqiao and Tieshan deposits are given in the Excel file. Supplementary data associated with this article can be found, in the online version, at http://dx.doi.org/10.1016/j.oregeorev.2017.07.019.

References

Balan, E., De Villers, J.P.R., Eeckhout, S.G., Glatzel, P., Toplis, M.J., Fritsch, E., Allard, T., Galoisy, L., Calas, G., 2006. The oxidation state of vanadium in titanomagnetite from layered basic intrusions. Am. Mineral. 91, 953–956.

Canil, D., Grondahl, C., Lacourse, T., Pisiak, L.K., 2016. Trace elements in magnetite from porphyry Cu–Mo–Au deposits in British Columbia, Canada. Ore Geol. Rev. 72, 1116–1128.

Carew, M.J., 2004. Controls on Cu–Au mineralization and Fe oxide metasomatism in the eastern fold belt. James Cook University, NW Queensland, Australia.

Chen, G.Y., Sun, D.S., Yin, H.A., 1987. Genetic Mineralogy and Prospecting Mineralogy. Chongqing Publishing House, Chongqing 356 pp. (in Chinese).

Chen, J.H., Zeng, J.N., Wang, S.Y., Li, J.W., Qiu, J.L., Zhang, Y., 2012. Characteristic of deposit geochemistry and discussion with metallogenic dynamics background of porphyite iron in Ningwu and Luzong volcanic basins. Geol. Sci. Technol Inf. 31, 86–94 (in Chinese with English abstract).

Chen, W.T., Zhou, M.F., Gao, J.F., Hu, R., 2015a. Geochemistry of magnetite from Proterozoic Fe–Cu deposits in the Kangdian metallogenic province, SW China. Mineral. Deposita 50, 795–809.

Chen, W.T., Zhou, M.F., Li, X., Gao, J.F., Hou, K., 2015b. In-situ LA-ICP-MS trace elemental analyses of magnetite: Cu–(Au, Fe) deposits in the Khetri copper belt in Rajasthan Province, NW India. Ore Geol. Rev. 65, 929–939.

Chung, D., Zhou, M.F., Gao, J.F., Chen, W.T., 2015. In-situ LA-ICP-MS trace elemental analyses of magnetite: the late palaeoproterozoic sokoman iron formation in the labrador trough, Canada. Ore Geol. Rev. 65, 917–928.

Dare, S.A.S., Barnes, S.J., Beaudoin, G., 2012. Variation in trace element content of magnetite crystallized from a fractionating sulfide liquid, Sudbury, Canada: implications for provenance discrimination. Geochim. Cosmochim. Acta 88, 27–50.

Dare, S.A., Barnes, S.J., Beaudoin, G., Méric, J., Boutroy, E., Potvin-Doucet, C., 2014. Trace elements in magnetite as petrogenetic indicators. Miner. Deposita 49, 785–796.

Duan, C., Li, Y.H., Yuan, S.D., Hu, M.Y., Zhao, L.H., Chen, X.D., Zhang, C., Liu, J.L., 2012. Geochemical characteristics of magnetite from Washan iron deposit in Ningwu ore district and its constraints on ore-forming. Acta Petrol. Sinica 28 (1), 243–257.

Duan, C., Zhou, T.F., Fan, Y., Yuan, F., Ding, M., Shang, S.G., Zhang, L.J., 2009. Geological characteristics of siderites from Longqiao iron deposit in Luzong volcanic basin and their genetic signif icance. Mineral Deposits 28, 643–652 (in Chinese with English abstract).

Duan, C., Mao, J.W., Li, Y.H., Hou, K.J., Yuan, S.D., Zhang, C., Liu, J.L., 2011. Zircon U-Pb geochronology of the gabbro–diorite porphyry and granodiorite porphyry from the Washan iron deposit in Ningwu Basin, and its geological significance. Acta Geol. Sinica 85, 1159–1171 (in Chinese with English abstract).

Duan, Z., Li, J.W., Hu, H., 2014. New constraints on the genesis of the Tieshan Fe–Cu skarn deposit, SE Hubei Province, China: textural and geochemical data of magnetite. Acta Geol. Sinica (English Ed.) 88 (Supp. 22), 1449–1450.

Dupuis, C., Beaudoin, G., 2011. Discriminant diagrams for iron oxide trace element fingerprinting of mineral deposit types. Mineral. Deposita. 46, 319–335.

Einaudi, M.T., Meinert, L.D., Newberry, R.J., 1981. Skarn deposits. Econ. Geol. 75, 317–391.

Fan, Y., Zhou, T.F., Yuan, F., Zhang, L.J., Qian, B., 2011. Geochronology of the porphyry-like type iron deposits in Ning–Wu basin: Evidence from 40Ar–39Ar phlogopite dating. Acta Geol. Sinica 85, 810–820 (in Chinese with English abstract).

Fan, Y., Liu, Y.N., Zhou, T.F., Zhang, L.J., Yuan, F., Wang, W.C., 2014. Geochronology of the Nihe deposit and in the Lu–Zong basin and its metallogenic significances. Acta Petrologica Sinica. 30, 1369–1381 (in Chinese with English abstract).

Huang, X.W., Gao, J.F., Qi, L., Meng, Y.M., Wang, Y.C., Dai, Z.H., 2016. In-situ LA-ICP-MS trace elements analysis of magnetite: The Fenghuangshan Cu–Fe–Au deposit, Tongling. Eastern China. Ore Geology Reviews. 72, 746–759.

Huang, X.W., Gao, J.F., Qi, L., Zhou, M.F., 2015a. In-situ LA-ICP-MS trace elemental analyses of magnetite and Re–Os dating of pyrite: The Tianhu hydrothermally remobilized sedimentary Fe deposit. NW China. Ore Geol. Rev. 65, 900–916.

Huang, X.W., Zhou, M.F., Qiu, Y.Z., Qi, L., 2015b. In-situ LA-ICP-MS trace elemental analyses of magnetite: The Bayan Obo Fe–REE–Nb deposit, North China. Ore Geol. Rev. 65, 884–899.

Huberty, J.M., et al., 2012. Silician magnetite from the Dales Gorge member of the Brockman iron formation, Hamersley Group, Western Australia. Am. Mineral. 97, 26–37.

Hu, H., Duan, Z., Luo, Y., Li, J.W., 2014a. Trace element systematics of magnetite from the Chengchao iron deposit in the Daye district: A laser ablation ICP-MS study and insights into ore genesis. Acta Petrol. Sinica 30, 1292–1306 (in Chinese with English abstract).

Hu, H., Li, J.-W., Lentz, D., Ren, Z., Zhao, X.-F., Deng, X.-D., Hall, D., 2014b. Dissolution–reprecipitation process of magnetite from the Chengchao iron deposit: insights into ore genesis and implication for in-situ chemical analysis of magnetite. Ore Geol. Rev. 57, 393–405.

Hu, H., Lentz, D., Li, J.W., McCarron, T., Zhao, X.F., Hall, D., 2015. Reequilibration processes in magnetite from iron skarn deposits. Econ. Geol. 110, 1–8.

Liang, H.Y., Sun, W., Su, W.C., Zartman, R.E., 2009. Porphyry copper-gold mineralization at Yulong, China, promoted by decreasing redox potential during magnetite alteration. Econ. Geol. 104, 587–596.

Li, J.W., Zeng, J.N., Xu, J.F., Qiu, H.N., Zhang, Y.X., Qin, Y.J., 2013. $^{40}Ar/^{39}Ar$ dating on phlogopite of Longqiao iron ore deposit in Lujiang, Anhui Province: The chronology evidence of ore genesis. Geol. Sci. Technol. Inf. 32, 171–180 (in Chinese with English abstract).

Lin, S.Z., 1982. A contribution to the chemistry, origin and evolution of magnetite. Acta Mineral. Sinica 2, 166–174 (in Chinese with English abstract).

Liu, P.P., Zhou, M.-F., Chen, W.T., Gao, J.-F., Huang, X.-W., 2015. In-situ LA–ICP–MS trace elemental analyses of magnetite: Fe–Ti–(V) oxide-bearing mafic–ultramafic layered intrusions of the Emeishan Large Igneous Province, SW China. Ore Geol. Rev. 65, 853–871.

Liu, Y., Hu, Z., Gao, S., Gunther, D., Xu, J., Gao, C., Chen, H., 2008. In situ analysis of major and trace elements of anhydrous minerals by LA-ICP-MS without applying an internal standard. Chem. Geol. 257, 34–43.

Ma, L.C., Dong, S.W., Zhong, Y.B., Zhang, Q.M., Gao, C.S., 2011. Metallogenic epoch of the Longqiao iron deposits at the Lujiang-Zongyang ore concentrated area in the Middle and Lower Reaches of Yangtze River, China. Acta Geol. Sinica 85, 1206–1214 (in Chinese with English abstract).

Makvandi, S., Beaudoin, G., McClenaghan, B.M., Layton-Matthews, D., 2015. The surface texture and morphology of magnetite from the Izok Lake volcanogenic massive sulfide deposit and local glacial sediments, Nunavut, Canada: Application to mineral exploration. J. Geochem. Explor. 150, 84–103.

McIntire, W.L., 1963. Trace element partition coefficients—a review of theory and applications to geology. Geochim. Cosmochim. Acta 27, 1209–1264.

Meinert, L.D., 1992. Skarns and skarn deposits. Geosci. Can. 19, 145–162.

Nadoll, P., Angerer, T., Mauk, J.L., French, D., Walshe, J., 2014a. The chemistry of hydrothermal magnetite: a review. Ore Geol. Rev. 61, 1–32.

Nadoll, P., Mauk, J.L., Leveille, R.A., Koenig, A.E., 2014b. Geochemistry of magnetite from porphyry Cu and skarn deposits in the southwestern United States. Mineral. Deposita. 50, 493–515.

Nadoll, P., Mauk, J.L., Hayes, T.S., Koenig, A.E., Box, S.E., 2012. Geochemistry of magnetite from hydrothermal ore deposits and host rocks of the Mesoproterozoic Belt Supergroup, United States. Econ. Geol. 107, 1275–1292.

Nielsen, R.L., Forsythe, L.M., Gallahan, W.E., Fisk, M.R., 1994. Major- and trace-element magnetite-melt equilibria. Chem. Geol. 117, 167–191.

Ni, R.S., Wu, Q.Q., Wang, X.Y., Wu, M.A., Zhang, Q.M., 1994. New data and evolutionary model of polymineralization for the Longqiao iron deposit, Lujiang, Anhui. Geol. Rev. 40, 565–576 (in Chinese with English abstract).

Nystroem, J.O., Henriquez, F., 1994. Magmatic features of iron ores of the Kiruna type in Chile and Sweden; ore textures and magnetite geochemistry. Econ. Geol. 89, 820–839.

Qu, H.Y., Wang, H.L., Pei, R.F., Yao, L., Wang, Y.L., Zheng, Z.G., 2012. Zircon U-Pb geochronological and Hf isotopic constraints on petrogenesis of Tieshan and Jinshandian plutons in the southeastern Hubei Province. Acta Petrol. Sinica 28, 147–165 (in Chinese with English abstract).

Ren, Q.J., Liu, X.S., Xu, Z.W., Qiu, D.T., Hu, W.X., Fang, C.Q., Ruan, H.C., Dong, H.G., Li, Z.L., Wu, Q.Z., 1991. Mesozoic volcano-tectonic depression and its mineralizing process in Lujiang-Zongyang area, Anhui province. Geological Press, Beijing 158 pp. (in Chinese).

Righter, K., Leeman, W.P., Hervig, R.L., 2006. Partitioning of Ni, Co and V between spinel-structured oxides and silicate melts: importance of spinel composition. Chem.

Geol. 227, 1–25.
Rudnick, R.L., Gao, S., 2003. The composition of continental crust. Treatise Geochem. 3, 1–64.
Rusk, B., Oliver, N., Brown, A., Lilly, R., Jungmann, D., 2009. Barren magnetite breccias in the Cloncurry region, Australia: comparisons to IOCG deposits. pp. 656–658.
Shen, J.C., Zeng, Y., Guo, K.Y., 2012. Discussions on division of Daye iron deposit as IOCG deposit. J. Geol. 36, 391–396 (in Chinese with English abstract).
Shu, Q.A., Chen, P.L., Cheng, J.R., 1992. The Geology of Iron and Copper Deposits in Eastern Hubei Province. Metallurgical Industry Press, Beijing (in Chinese).
Singoyi, B., Danyushevsky, L, Davidson, G.J., Large, R., Zaw, K., 2006. Determination of trace elements in magnetites from hydrothermal deposits using the LA-ICP-MS technique. Abstracts of Oral and Poster Presentations from the SEG 2006 Conference Society of Economic Geologist, Keystone, USA, pp. 367–368.
Sun, Y.D., Yang, R.Y., Ren, Q.J., Liu, X.S., 1994. Discussion on the characteristics and tectonic setting of the Mesozoic volcanic sequences in Lujiang-Zongyang area. Acta Geol. Sinica 10, 94–103 (in Chinese with English abstract).
Takeno, N., 2005. Atlas of Eh-pH diagrams: Intercomparison of thermodynamic data bases. Geol. Survey Jpn Open File Rep. 419, 285.
Tang, Y.C., 1998. The Geology of Copper-Gold Polymetallic Ore Deposits Along the Yangtze River in Anhui Province. Geological Press, Beijing (in Chinese).
Toplis, M.J., Corgne, A., 2002. An experimental study of element partitioning between magnetite, clinopyroxene and iron-bearing silicate liquids with particular emphasis on vanadium. Contrib. Mineral. Petrol. 144, 22–37.
Tosdal, R.M., Dilles, J.H., Cooke, D.R., 2009. From source to sinks in auriferous magmatichydrothermal porphyry and epithermal deposits. Elements 5, 289–295.
Wang, M.F., Wang, W., Liu, K., Michalak, P.P., Wei, K.T., Hu, M.Y., 2016. In-situ LA-ICP-MS trace elemental analyzes of magnetite: The Tieshan skarn Fe–Cu deposit, Eastern China. Chemie der Erde. 77 (1), 169–181.
Wang, Q., Wyman, D.A., Xu, J.F., Zhao, Z.H., Jian, P., Xiong, X.L., Bao, Z.W., Li, C.F., Bai, Z.H., 2006. Petrogenesis of Cretaceous adakitic and shoshonitic igneous rocks in the Luzong area, Anhui Province (eastern China): Implications for geodynamics and Cu–Au mineralization. Lithos 89, 424–446.
Wang, W., Wang, M.F., Guo, X.N., Wei, T., Ke, F.M., Hu, M.Y., Liu, K., 2015. Geochemical characteristics of cagnetite elements in the Tieshan iron deposit in southeastern Hubei province and geological implications. Geol. Explor. 51 (3), 451–465.
Williams, P.J., Barton, M.D., Johnson, D.A., Fontbote, L., Haller, A.D., Mark, G., Oliver, N. H.S., Marschik, R., 2005. Iron oxide copper-gold deposits: Geology, space-time distribution, and possible modes of origin. Economic Geology 100th Anniversary Volume, 2005. pp. 371–405.
Wu, M.A., 1996. Longqiao Iron Ore Deposit in Anhui Province. Geological Press, Beijing (in Chinese).
Xie, G.Q., Mao, J.W., Li, R.L., Zhao, H.J., 2006. Geological characteristics and mineral model of skarn Fe deposits from southeastern Hubei Province. China. Mineral Deposits. 25, 147–150.
Xie, G.Q., Mao, J.W., Zhao, H.J., Duan, C., Yao, L., 2012. Zircon U-Pb and phlogopite ^{40}Ar-^{39}Ar age of the Chengchao and Jinshandian skarn Fe deposits, southeast Hubei Province, Middle-Lower Yangtze River Valley metallogenic belt, China. Mineral Deposits. 47, 633–652.
Xie, G.Q., Mao, J.W., Zhu, Q.Q., Yao, L., Li, Y.H., Li, W., Zhao, H.J., 2015. Geochemical constraints on Cu–Fe skarn deposits in the Edong district, Middle-Lower Yangtze River metallogenic belt, China. Ore Geol. Rev. 64, 425–444.
Xue, H.M., Dong, S.W., Ma, F., 2010. Geochemistry of shoshonitic volcanic rocks in the Luzong Basin, Anhui Province (Eastern China): Constraints on Cretaceous lithospheric thinning of the Lower Yangtze Region. Acta Geol. Sinica 84, 664–681 (in Chinese with English abstract).
Yao, P.H., Wang, K.N., Du, C.L., Lin, Z.T., Song, X., 1993. Records of Chinese Iron Ore Deposits. Metallurgic Industry Press, Beijing (in Chinese).
Zeng, J.N., Qin, Y.J., Guo, K.Y., Chen, G.G., Zeng, Y., 2010. Zircon U-Pb dating of ore-bearing magmatic rocks and its constraint on the formation time of the ore deposits in Luzong Basin. Anhui Province. Acta Geologica Sinica. 84, 466–478 (in Chinese with English abstract).
Zhai, Y.S., Shi, Z.L., Lin, X.D., Xiong, P.F., Wang, D.Y., Yao, S.Z., Jin, Z.M., 1982. Genesis of “Daye Type” iron ore deposits in eastern Hubei, China. Earth Sci. – J/ Wuhan College of Geol. 3, 239–251 (in Chinese with English abstract).
Zhai, Y.S., Yao, S.Z., Lin, X.D., Zhou, X.R., Wan, T.F., Zhou, Z.G., 1992. Metallogenic regularity of iron and copper deposits in the Middle and Lower Valley of the Yangtze River. Mineral Deposits. 11 (1), 1–12 (in Chinese with English abstract).
Zhai, Y.S., Xiong, Y.L., Yao, S.Z., Lin, X.D., 1996. Metallogeny of copper and iron deposits in the Eastern Yangtze Craton, east-central China. Ore Geol. Rev. 11, 229–248.
Zhang, S., Wu, M.A., Zhao, W.G., Zhang, Y.Y., Li, X.D., Wang, J., 2014. Geochemistry characteristics of Nihe iron deposit in Lujiang, Anhui Province and their constrains to ore genesis. Acta Petrol. Sinica 30, 1382–1396 (in Chinese with English abstract).
Zhao, A.X., 1990. A study on the mineral chemistry of magnetite from Tieshan iron-copper mineral deposit, Daye, Hubei and its origin. Earth Science-Journal of China University of Geosciences. 15, 385–396 (in Chinese with English abstract).
Zhao, L.D., Chen, H.Y., Zhang, L., Li, D.F., Zhang, W.F., Wang, C.M., Yang, J.T., Yan, X.L., 2016. Magnetite geochemistry of the Heijianshan Fe–Cu (–Au) deposit in Eastern Tianshan: Metallogenic implications for submarine volcanic-hosted Fe–Cu deposits in NW China. Ore Geol. Rev. http://dx.doi.org/10.1016/j.oregeorev.2016.07.022.
Zhao, W.W., Zhou, M.F., 2015. In-situ LA-ICP-MS trace elemental analyses of magnetite: The Mesozoic Tengtie skarn Fe deposit in the Nanling Range. South China. Ore Geol. Rev. 65, 872–883.
Zhou, T.F., Fan, Y., Yuan, F., Lu, S.M., Shang, S.G., David, C., Sebastien, M., Zhao, G.C., 2008a. Geochronology of the volcanic rocks in the Lu–Zong Basin and its significances. Sci. China (Series D). 38 (10), 1342–1353.
Zhou, T.F., Fan, Y., Yuan, F., 2008b. Advances on petrogensis and metallogeny study of the mineralization belt of the Middle and Lower Reaches of the Yangtze River area. Acta Petrol. Sinica 24, 1665–1678 (in Chinese with English abstract).
Zhou, T.F., Fan, Y., Yuan, F., Song, C.Z., Zhang, L.J., Qian, C.C., Lu, S.M., David, R.C., 2010. Temporal–spatial framework of magmatic intrusions in Luzong volcanic basin in East China and their constrain to mineralizations. Acta Petrol. Sinica 26, 2694–2714 (in Chinese with English abstract).
Zhou, T.F., Wu, M.A., Fan, Y., Duan, C., Yuan, F., Zhang, L.J., Liu, J., Qian, B., Franco, P., David, R.C., 2011. Geological, geochemical characteristics and isotope systematics of the Longqiao iron deposit in the Lu–Zong volcano-sedimentary basin, Middle-Lower Yangtze (Changjiang) River Valley, Eastern China. Ore Geol. Rev. 43, 154–169.